UNIVERSITY OF CALIFORNIA
RIVERSIDE

Analysis of Innovative Heat Sinks in Electronic Cooling Applications

A Dissertation submitted in partial satisfaction
of the requirements for the degree of

Doctor of Philosophy

in

Mechanical Engineering

by

Khavar Fazeli

September 2023

Dissertation Committee:
Dr. Kambiz Vafai, Chairperson
Dr. Heejung Jung
Dr. Cengiz Ozkan

The Dissertation of Khavar Fazeli is approved:

Committee Chairperson

University of California, Riverside

Dedicated to

My beloved mother, whose memory and love continue to inspire me every day.

ABSTRACT OF THE DISSERTATION

Analysis of Innovative Heat Sinks in Electronic Cooling Applications

by

Khavar Fazeli

Doctor of Philosophy, Graduate Program in Mechanical Engineering
University of California, Riverside, September 2023
Dr. Kambiz Vafai, Chairperson

Managing the heat generated in electronic components has always been a challenge. As these devices get more compact and powerful, efficient thermal management is crucial to ensure the reliability, performance, and lifespan of electronic components. In this work, innovative heat sink designs consisting of Microchannel Heat Sinks (MCHS) and Flat Plate Micro Heat Pipes (FPM-HP) are investigated to improve thermal management in electronic components. The three-dimensional finite volume method is used to analyze the fluid flow and heat transfer in the heat sinks. The validity of the numerical models is confirmed by comparison with pertinent experimental data. The thermal performances of the new heat sink designs are compared to that of double-layer microchannel heat sinks with parallel flow (DLPF MCHS) and counter flow (DLCF MCHS) configurations, as two of the more efficient heat sink designs in the industry.

This study first focuses on optimizing MCHS designs for electronic cooling applications with constant heat flux at the base. MCHSs with rectangular and triangular cross-sections and counter flow arrangement in adjacent channels (Counter Dual MCHSs) are thoroughly investigated. The investigated configuration of Silicon-Water Counter Dual MCHS with rectangular cross-section improves the temperature uniformity by 43-50% and 26-31% compared to DLPF and DLCF MCHSs, respectively, and the triangular cross-section configuration improves it by 38-47% and 21-26%, respectively. The thermal resistance of heat sinks is reduced by 10-15% compared to DLPF MCHS and by 2-8% compared to DLCF MCHS.

Additionally, innovative hybrid heat sink designs combined with MCHS and FPM-HP are proposed to optimize hotspot management in electronics cooling applications that involve local high heat generation. The hybrid DLPF MCHS & FPM-HP reduces the maximum temperature and surface temperature gradient of the heat sink by 13-23% and 20-49%, while these are reduced by 16-40% and 27-64% for the hybrid DLCF MCHS & FPM-HP compared with the corresponding copper base (no heat pipe) designs. The hybrid Counter Dual Rectangular MCHS & FPM-HP reduces the maximum temperature and surface temperature gradient of the heat sink by 15-24% and 29-65% compared with the DLCF MCHS with copper base (no heat pipe) design, while these are reduced by 10-26% and 24-63% for the Counter Dual Triangular MCHS, respectively.

Table of Contents

List of Figures

List of Tables

Nomenclature

$\vec{V}$: velocity, m/s

T: temperature, K

ρ: density, kg/m^3

p: pressure, Pa

μ: dynamic viscosity, N.s/m^2

Nu: Nusselt number

h: heat transfer coefficient, W/m^2.K

d_H: hydraulic diameter, m

k: thermal conductivity, W/m.K

k_{eff}: effective thermal conductivity, W/m.K

C_p: specific heat at constant pressure, J/kg.K

f: Darcy friction factor

Re: Reynolds number

R_T: thermal resistance, K/W

q'': heat flux, W/m^2

A: area, m^2

$\dot{m}$: mass flow rate, kg/s

h_{fg}: latent heat of evaporation, J/kg

ε: porosity

K: permeability

AR: aspect ratio

Subscript

f: fluid

g: gas

l: liquid

s: solid

v: vapor

Chapter 1: Introduction and Background

1.1. The Significance of Thermal Management in Electronic Devices

Dissipation of heat created in electronic components has always been a challenge. As electronic devices get more compact and powerful, the need for effective thermal management systems becomes even more crucial. In 1965, Gordon E. Moore predicted that the density of transistors and components per integrated circuit would double every two years, leading to more heat generation [1].

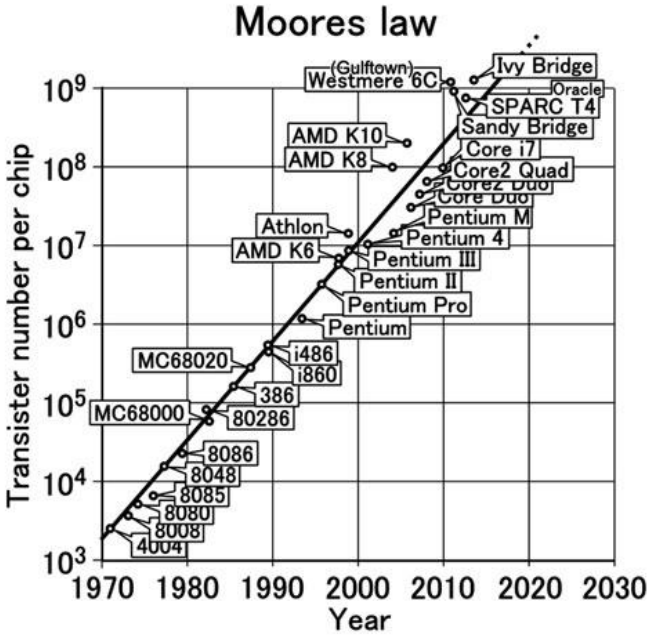

Figure 1-1 Gordon E. Moore predicted that the density of transistors per integrated circuit doubles every two years. Moore's law remains valid after 50 years (This image is available in the public domain and created by shigeru23, CC BY-SA).

The heat created in electronic devices has increased significantly over the years, reaching up to 100-1000 W/cm^2, which is comparable to the heat flux experienced in nuclear reactors and the ballistic entry [2]. Even though rocket heat shields and nuclear

blast targets can reach temperatures exceeding 1000°C, to ensure reliability of microelectronic components operating in the same heat flux range, maximum chip surface temperatures must be kept below 100°C. Without proper thermal management systems, the heat generated by these devices can cause significant temperature rises that can impact their performance and reliability. To ensure optimal functionality, it is essential to remove the generated heat effectively with lower temperature rise and uniform temperature distribution within the electronic component.

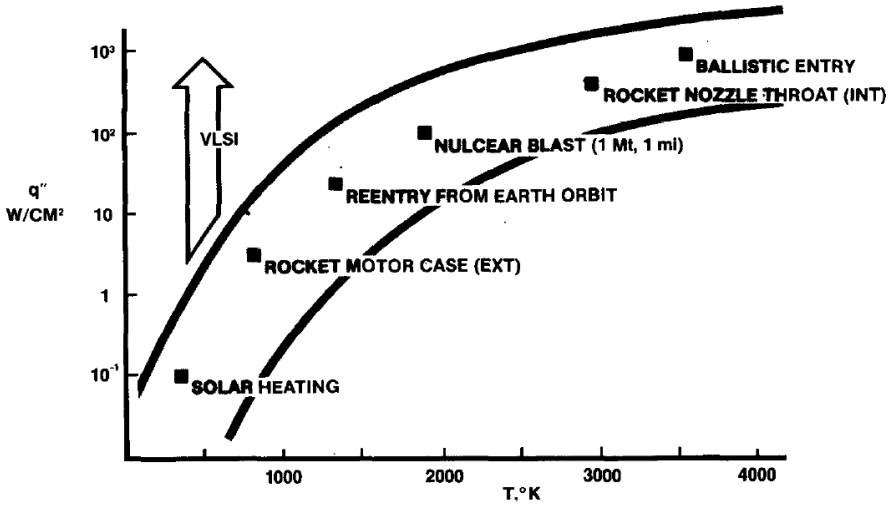

Figure 1-2 Magnitude of heat generated in microelectronic [2].

1.2. Microchannel Heat Sinks

1.2.1 Introduction

A microchannel heat sink is a compact, high-performance cooling solution that is commonly used in applications where space is limited. The heat sink consists of a series of microchannels that are etched into a metal or ceramic substrate. These channels are typically less than 1 mm in width and depth, and they are designed to increase the surface area of the heat sink, allowing for more efficient heat transfer. The microchannels are often

filled with a coolant, such as water or a refrigerant, which helps to absorb and dissipate the heat generated by the electronic device. The cooling fluid flows through the micro-scale channels, picking up the dissipated heat. Overall, microchannel heat sinks are highly effective cooling solutions for a wide range of electronic applications.

Figure 1-3 Image of a chip with an integrated microchannel cooling system developed by Swiss Federal Institute of Technology in Lausanne (This image is available in the public domain, Credit: Copyright © Alain Herzog EPFL).

1.2.2 Background

The first microchannel heat sink was introduced by Tuckerman and Pease in 1981 [3] and was considered a milestone in heat sink technology. Many studies have been conducted to improve the thermal and hydraulic performance of MCHS. One of the most significant innovations in MCHS design is double-layer and multi-layer MCHSs, first established by Vafai and Zhu [4-6]. Vafai and Zhu [4] demonstrated that utilizing two layers of MCHS with counter flow configuration on top of each other decreases the stream-wise temperature rise dramatically compared to regular single-layer MCHS. It also offers

a more uniform temperature distribution. Many other numerical and experimental studies have shown that double- and multi-layer MCHS designs have higher thermal capability than single-layer ones. Wei and Joshi [7] investigated multi-layer MCHS with flexible control over each layer's flow direction and flow rate. This study indicates that multi-layer MCHSs are more efficient regarding pumping power requirements. Patterson et al. [8] numerically investigated the heat transfer inside stacked microchannels with different flow arrangements. They reported that the counter flow arrangement proved to have the most uniform temperature distribution for the range of flow rates they studied. In contrast, the parallel flow configuration performs best in reducing the peak temperature. The same results were reported by Wei et al. [9,10]. Levac et al. [11] investigated the effect of Reynolds number, inlet velocity profile, and flow configuration in the channels of the MCHS. They found that within the range $116 \leq Re \leq 1160$, the two-layer MCHS with counter flow has the lowest peak temperature, while the peak temperature in parallel flow arrangement is lower at Re <~ 100. Wong and Muezzin [12] also established that counter flow configuration is superior to parallel flow for high Reynolds numbers. Regarding the uniformity of temperature on the chip, the counter flow arrangement performed better than parallel flow at all values of Re. Lin et al. [13, 14] performed a thorough parametric investigation on double and multi-layer MCHS to better understand the design factors concerning channel dimensions, pumping power distribution, and flow configuration. They established that the optimized flow configuration is (0,1), (0,1,1), (0,1,1,1), respectively, for two-, three- and four-layer MCHSs ('0' stands for flow in positive x-direction and '1' stands for flow in negative x-direction). Their result shows that the counter flow

arrangement is more effective when applied to the first two layers of channels. Lu and Vafai [15] thoroughly compared innovative MCHSs, including two-layer and multi-layer MCHS, showing that double-layer and multi-layer MCHS have lower thermal resistance and temperature gradient, and require less pumping power.

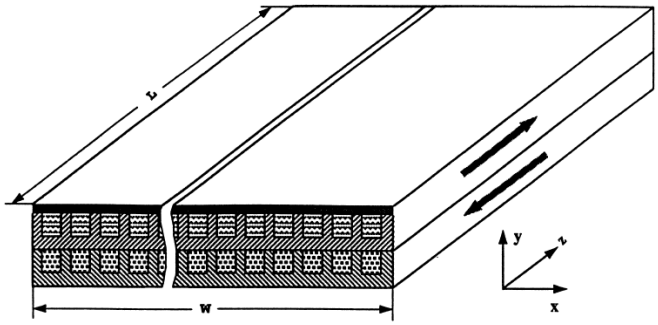

Figure 1-4 Schematic view of Double-Layer Counter flow MCHS introduced by Vafai and Zhu [4-6].

The effect of the flow regime on single-layer and double-layer MCHSs was studied by Chong et al. [16]. Their research indicates that for a fixed pressure drop, both optimized heat sinks operating in the laminar regime perform better than under turbulent flow conditions. Some researchers have examined the effectiveness of multi-layering in MCHSs made of materials other than silicon. Skandakumaran et al. [17] conducted a modeling and experimental study of multi-layered MCHS made of SiC. They established that multi-layer heat sinks made of silicon carbide have lower thermal resistance than single layer samples. In another study, Skandakumaran and Ortega [18] experimentally showed that multilayer MCHS made of copper has significant advantages over single-layer equivalents with reduced thermal resistance and pressure drop. Saidi and Khiabani [19] have shown that multilayering microchannels is more effective when using solid materials with high thermal conductivity. Hung et al. [20] have shown that a coolant with high thermal

conductivity and specific heat, and low dynamic viscosity enhances the thermal performance of MCHSs.

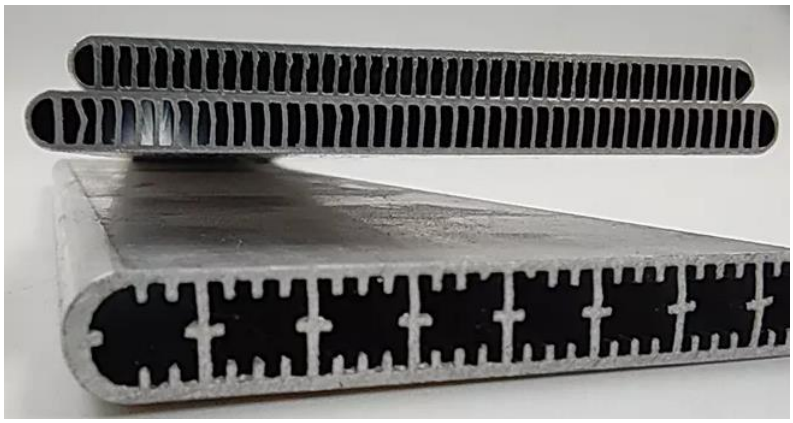

Figure 1-5 Microchannel tube manufactured for automotive battery heat sink, by Trumony Aluminum Limited, China (This image is available in the public domain).

Some other innovative designs have been proposed to enhance the performance of MCHSs. Bau [21] offered a MCHS with varying channels cross-sectional area in the axial direction. But, a high pressure drop is expected in their design due to increasing the flow velocity along the channel. Cheng [22] numerically investigated applying passive microstructure to enhance mixing in the stacked two-layer microchannel heat sink. Morshed and Khan [23] numerically investigated interconnected vertical channels to allow a cross-flow of the coolant in multi-layered MCHS. They reported a significant improvement in thermal resistance for multiple layers. The cross-flow between the channels discupts the boundary layer of the coolant and improves heat sink's thermal performance. This design is more effective for heat sinks with a low thermal conductivity material. Hung et al. [20] have shown that an increased channel aspect ratio reduces the pressure drop. Chuan et al. [24] proposed double-layered microchannel heat sink with truncated top channels, which reduced the thermal resistance by 37.5% in comparison to

the original design. For a double-layered MCHS with the counter-flow arrangement, there is a negative heat flux from the fluid to the adjacent solid in regions close to the outlet of second layer channels, specifically in low Reynolds numbers [11, 12, 25]. The proposed design by Chuan et al. [24] with truncated top channels minimizes this negative heating effect. Vafai and Khaled [26] investigated new flexible single-layer and double-layer MCHSs. They found that double-layer flexible MCHSs improves the cooling rate copared to single layer flexible MCHSs at a low pressure drop ranges. In another study, Khaled and Vafai [27] used rotatable plates to separate the layers in double-layered microchannels to increase the cooling in MCHS. They found that double layer flexible MCHS with a rotatable plate has higher cooling rate than an equivalent rigid one at specific range of Reynolds number, stiffness, and aspect ratios.

1.3 Heat Pipes

1.3.1 Introduction

A heat pipe is a vacuum sealed metal tube with a thin wick layer on the internal surface. It contains a working fluid that circulates within the device and transfers heat from hot spots to cooler regions. When heat is introduced to a section of the heat pipe, called the evaporator section, the working fluid evaporates, and the hot vapor travels to the colder region, called the condenser section, where it condenses back to liquid. The capillary action forces the condensed liquid to travel back from the condenser to the evaporator section through the wick's porous structure [28]. The phase change allows the heat pipe to provide efficient and uniform cooling across large surfaces without needing external power input or moving parts. Heat pipe transfer heat much more efficiently than solid metal with a

significantly lighter weight. They can also be combined with other cooling methods for additional thermal management.

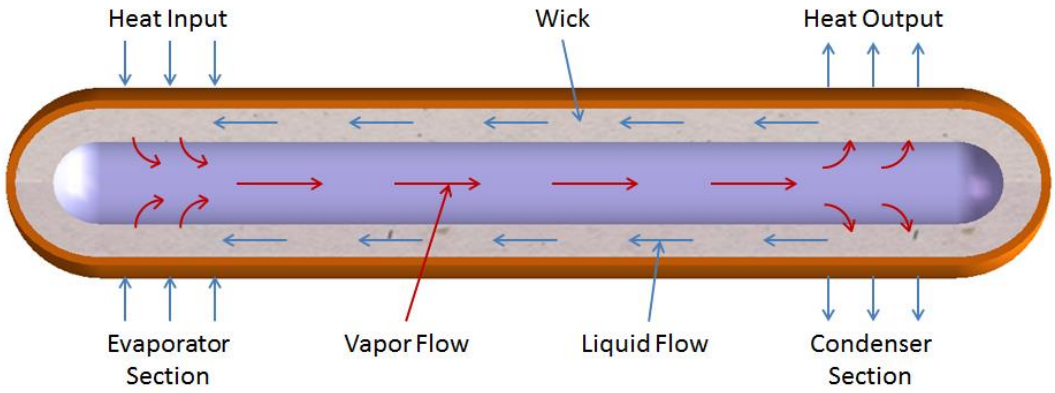

Figure 1-6 Heat pipe working principle (This image is available in the public domain and provided by MyHeatSinks, Inc., China).

1.3.2 Background

The history of heat pipes dates back to 1942 when R.S. Gaugler introduced the concept. However, it wasn't until the 1960s when advanced materials and manufacturing techniques were developed that heat pipes gained prominence. G. Grover's groundbreaking work on capillary-driven heat transfer in wicks and evaporator-condenser configurations laid the foundation for modern heat pipe technology. The use of heat pipes in electronic cooling gained significant attention in the 1970s and 1980s due to the challenges faced by the semiconductor industry in dissipating the increasing heat loads generated by integrated circuits (ICs). Heat pipes find extensive application in various electronic cooling scenarios, including CPUs, GPUs, LED lighting, power electronics, and mobile devices. Traditional heat pipes are limited by their round shape, which makes it challenging to provide an effective cooling surface on smaller heat sources. Multi-channel Flat shaped heat pipes, established and investigated by Vafai et al. [29-33], overcome these limitations by

providing better geometric adaptability and the ability to operate reliably under asymmetrical heat load conditions.

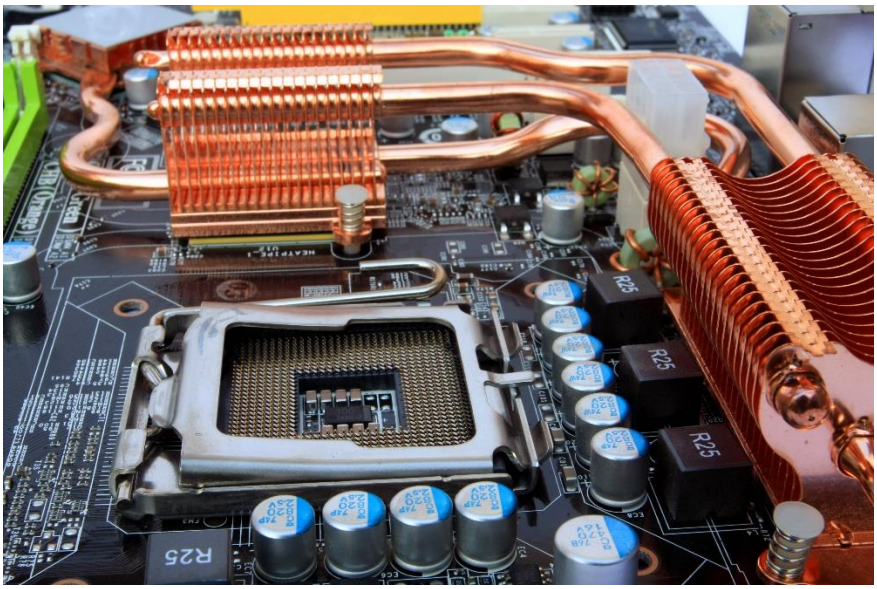

Figure 1-7 An example of a combination of heat pipes in electronic cooling application (This image is available in the public domain and provided by DNP (Dai Nippon Printing Co., Ltd.), Tokyo, Japan.).

Pulsating heat pipes, which rely on the coolant's phase change within the pipes, are among the top cooling methods in electronics [34,35]. Noh and Kim [36] conducted thermal optimization on pulsating heat pipes (PHPs) using numerical methods. Their research focused on a one-dimensional numerical model that sumulated physical processes occurring in a PHP. They found that there is an optimal channel diameter or number of turns for the thermal efficiency of a PHP in a vertical position under the constraint of limited space.

There have been some major advancements in microfabrication techniques that have led to the creation of miniature and micro heat pipes. Micro heat pipes are specifically designed to offer enhanced thermal management capabilities in small-scale applications,

such as microelectronics, medical devices, portable devices, and aerospace. Miniature heat pipes with a diameter of 2-3 mm have been utilized in smartphone applications (Fujikura Electronics (Thailand) Ltd.). These heat pipes contain a sintered fiber wick within their walls, with the copper fiber bundle wick being a popular choice due to its high capilarity characteriztics and permeability. Additionally, the copper metal fiber wick has a higher thermal conductivity, making it an excellent option [37, 38]. Zhu and Vafai [39-42] have developed a detailed analytical model for asymmetrical flat-shaped heat pipes, which includes both cases of flat-plate and disc-shaped variants. Their model predicts the maximum heat transfer capability with high accuracy, using a pseudo-three-dimensional approach. According to Vafai and colleagues [33, 43], the thickness of the wick and vapor channel can have an impact on the thermal performance of flat-shaped heat pipes. Their study found that the heat transfer capability of disk-shaped heat pipes with a smaller surface was significantly higher than that of rectangular flat-plate heat pipes. In another study by Vadakkan et al. [44], the performance of a flat heat pipe with multiple heat sources was analyzed using numerical methods. The analysis included solving 3D flow and energy equations, as well as accounting for conduction in the wall for both the vapor and wick regions. A solution for liquid and vapor flows within a flat micro heat pipe, along with the temperature inside the heat pipe wall, was presented by Lefevre and Lallemand [45]. Their work highlighted the significance of accounting for pressure drop in vapor flow and axial wall conduction, particularly for heat pipes with high thermal conductivity.

Researchers are exploring the integration of micro heat pipes with other thermal management techniques, such as microfans, micro pumps, or thermoelectric devices, to

enhanced heat transfer capabilities and efficiency. This combination of techniques is referred to as hybrid systems, and it holds great promise in improving the performance and reliability of electronic devices. In this study, innovative combined Heat Sink designs that utilize MCHS and Flat Plate Micro Heat Pipe (FPM-HP) is introduced. This hybrid design is particularly beneficial for managing hotspots in electronic cooling applications that involve local high heat generation. Combining these two technologies can achieve optimal cooling performance and ensure that the electronic device operates efficiently.

References

[1] Moore, Gordon E., “Cramming more components onto integrated circuits”, Proceedings of the IEEE, Vol. 86, No. 1 (1998).

[2] A. Bar Cohen, “Thermal Management of Air- and Liquid-Cooled Multichip Modules”, IEEE Transactions on Components, Hybrids, and Manufacturing Technology, Vol. CHMT-10, No. 2 (1987).

[3] Tuckerman, D. B, Pease, R. F. W., “High-Performance Heat Sinking for VLSI”, Electron Device Letters, IEEE 2.5 (1981): 126 -129.

[4] Vafai, K., Zhu, L., “Analysis of two-layered micro-channel heat sink concept in electronic cooling”, International Journal of Heat and Mass Transfer (1999), 42: 2287-2297.

[5] Vafai, K., Zhu, L., “Two-layered micro-channel heat sink, devices and systems incorporating same”, U.S. Patent No. 6,457,515. 1 (2002).

[6] Vafai, K., Zhu, L., “Multi-layered micro-channel heat sink, devices and systems incorporating same”, U.S. Patent No. 6,675,875. 13 (2004).

[7] Wei, X., Joshi, Y., “Optimization study of stacked micro-channel heat sinks for micro-electronic cooling”, Components and Packaging Technologies, IEEE Transactions on 26.1 (2003): 55-61.

[8] Patterson, M. K., Wei, X., Joshi, Y., Prasher, R., “Numerical study of conjugate heat transfer in stacked microchannels”, Thermal and Thermomechanical Phenomena in Electronic Systems (2004), ITHERM'04. The Ninth Intersociety Conference on. IEEE.

[9] Wei, X., Joshi, Y., “Stacked microchannel heat sinks for liquid cooling of microelectronic components”, Journal of Electronic Packaging 126.1 (2004): 60-66.

[10] Wei, X., Joshi, Y., Patterson, M. K., “Stacked Microchannel Heat Sinks for Liquid Cooling of Microelectronics”, ASME International Mechanical Engineering Congress and Exposition. American Society of Mechanical Engineers (2004).

[11] Levac, M. L.-J., Soliman, H. M., Ormiston, S. J., “Three-dimensional analysis of fluid flow and heat transfer in single- and two-layered micro-channel heat sinks”, Heat and mass transfer 47.11 (2011): 1375-1383.

[12] Wong, K. C., Muezzin, F. N. A., “Heat transfer of a parallel flow two-layered microchannel heat sink”, International Communications in Heat and Mass Transfer (2013), 49: 136-140.

[13] Lin, L., Chen, Y.-Y., Zhang, X.-X., Wang, X.-D., “Optimization of geometry and flow rate distribution for double--layer microchannel heat sink”, International Journal of Thermal Sciences (2014), 78: 158-168.

[14] Lin, L., Deng, M.-X., Zhang, X.-X., Wang, X.-D., “Numerical analysis and parametric study of multilayered microchannel heat sinks”, Advances in Mechanical Engineering (2015), Vol. 7(7) 1–10.

[15] Lu, S., Vafai, K., “A comparative analysis of innovative microchannel heat sinks for electronic cooling”, International Communications in Heat and Mass Transfer (2016), 76: 271–284.

[16] Chong, S. H., K. T. Ooi, and T. N. Wong. "Optimisation of single- and double-layer counter flow microchannel heat sinks." Applied Thermal Engineering 22.14 (2002): 1569-1585.

[17] Skandakumaran, P., et al. "Multi--layered SiC microchannel heat sinks-- modeling and experiment." Thermal and Thermomechanical Phenomena in Electronic Systems, 2004. ITHERM'04. The Ninth Intersociety Conference on. IEEE (2004).

[18] Lei, N., P. Skandakumaran, and A. Ortega. "Experiments and modeling of multilayer copper minichannel heat sinks in single--phase flow." Thermal and Thermomechanical Phenomena in Electronics Systems (2006), ITHERM'06. The Tenth Intersociety Conference on IEEE.

[19] Saidi, M. H., and Reza H. Khiabani. "Forced convective heat transfer in parallel flow multilayer microchannels." Journal of Heat Transfer 129.9 (2007): 1230-1236.

[20] Hung, Tu-Chieh, Wei--Mon Yan, and Wei--Ping Li. "Analysis of heat transfer characteristics of double--layered microchannel heat sink." International Journal of Heat and Mass Transfer 55.11 (2012): 3090-3099.

[21] Bau, H. H., “Optimization of conduits shape in micro-heat exchangers”, Int. J. Heat Mass Transfer 41 (1998) 2717– 2723.

[22] Cheng, Y. J. "Numerical simulation of stacked microchannel heat sink with mixing--enhanced passive structure." International communications in heat and mass transfer 34.3 (2007): 295-303.

[23] Morshed, A. K. M. M., and Jamil A. Khan. "Numerical analysis of single phase multi layered micro--channel heat sink with inter--connects between vertical channels." 2010 14th International Heat Transfer Conference. American Society of Mechanical Engineers (2010).

[24] Leng, C., Wang, X.-D., Wang, T.-H., Yan, W.-M., “Multi--parameter optimization of flow and heat transfer for a novel double layered microchannel heat sink.” International Journal of Heat and Mass Transfer 84 (2015): 359-369.

[25] Wei, X., Joshi, Y., Patterson, M. K., “Experimental and numerical study of a stacked microchannel heat sink for liquid cooling of microelectronic devices”, Journal of Heat Transfer 129.10 (2007): 1432-1444.

[26] K. Vafai, A. Khaled, “Analysis of flexible micro-channel heat sink systems”, International Journal of Heat and Mass Transfer 48 (2005) 1739–1746

[27] A. Khaled, K. Vafai, “Cooling augmentation using microchannels with rotatable separating plates”, International Journal of Heat and Mass Transfer 54 (2011) 3732–3739, US Patent # 7, 654,468.

[28] Zohuri, B., “Heat Pipe Design and Technology”, Modern Application for Practical Thermal Management, Second Edition, Springer, (2016).

[29] Vafai, K., and Wang, W., “Analysis of Flow and Heat Transfer Characteristics of an Asymmetrical Flat Plate Heat Pipe”, Int. J. Heat Mass Transfer (1992), Vol. 35(9), pp. 2087–2099.

[30] Vafai, K., Zhu, N., and Wang, W., “Analysis of Asymmetric Disk-Shaped and Flat-Plate Heat Pipes”, ASME J. Heat Transfer-Trans. (1995), 117(1), pp. 209–218.

[31] Wang, Y., Vafai, K., “An Experimental Investigation of the Thermal Performance of an Asymmetrical Flat Plate Heat Pipe”, Int. J. Heat Mass Transfer (2000), 43(15), pp. 2657–2668.

[32] Zhu, N., Vafai, K., “Vapor and Liquid Flow in an Asymmetrical Flat Plate Heat Pipe: A Three-Dimensional Analytical and Numerical Investigation”, Int. J. Heat Mass Transfer (1998), 41(1), pp. 159–174.

[33] Vafai, K., and Zhu, N., “Closure to “Analysis of Asymmetric Disk-Shaped and Flat-Plate Heat Pipes”, ASME J. Heat Transfer-Trans. (2014), 136(11), p. 116001.

[34] V. S. Nikolayev, “Physical principles and state-of-the-art of modeling of the pulsating heat pipe: a review,” Appl. Therm. Eng., vol. 195, p. 117111 (2021).

[35] M. Ahmadian-Elmi,M. R. Hajmohammadi,S. S Nourazar,K. Vafai &M. B. Shafii, “Effect of filling ratio, number of loops, and transverse distance on the performance of pulsating heat pipe in a microchannel heat sink”, Numerical Heat Transfer (2023).

[36] H. Y. Noh and S. J. Kim, “Numerical simulation of pulsating heat pipes: Parametric investigation and thermal optimization,” Energy Convers. Manag., vol. 203, p. 112237 (2020).

[37] Ru J, Kong B, Zhu H, Shi Z, Zhang D, Fan T., “Microstructure, capillary performance and gas permeability of Biporous copper fabricated by tape casting”, Powder Technol 256:182–187 (2014).

[38] Maneemuang, S., Vafai, K., Kammuang-Lue1, N., Terdtoon, P., Sakulchangsatjatai, P., “Analysis of the optimum configuration for the capillary rise and the permeability of the fiber wick structure for heat removal in heat pipes”, Heat and Mass Transfer (2021) 57:1513–1526.

[39] Zhu, N., Vafai, K., “Optimization of asymmetrical disk-shaped heat pipes”, AIAA. J Thermophys Heat Transfer (1996) 10:179–182.

[40] Zhu, N., Vafai, K., “The effects of liquid-vapor coupling and non-Darcian transport on asymmetrical disk-shaped heat pipes”, Int J Heat Mass Transf (1996), 39:2095–2113.

[41] Zhu, N., Vafai K., “Numerical and analytical investigation of vapor flow in a disk-shaped heat pipe incorporating secondary flow”, Int J Heat Mass Transf (1997), 40:2887–2900.

[42] Zhu, N., Vafai, K., “Analytical modeling of the startup characteristics of asymmetrical flat-plate and disk-shaped heat pipes”, Int J Heat Mass Transf (1998) 41:2619–2637.

[43] Vafai, K., Zhu, N., Wang, W., “Analysis of asymmetric disk shaped and flat plate heat pipes”, ASME J Heat Transfer (1995) 117:209–218.

[44] Vadakkan, U., Garimella, S.V., Murthy, J.Y., “Transport in flat heat pipes at high heat fluxes from multiple discrete sources”, ASME J. Heat Transfer (2004), No. 126, pp. 347-354.

[45] Lefèvre, F., Lallemand, M., “Coupled thermal and hydrodynamic models of flat micro heat pipes for the cooling of multiple electronic components”, Int. J. Heat Mass Transfer (2006), No. 49, pp. 1375-1383.

Chapter 2: MCHS designs with counter flow arrangement in adjacent channels.

2.1. Introduction

In applications with high cooling capacity and packing density requirements, contained liquid-forced cooling is one of the attractive choices. An effective cooling method is to mount a microchannel heat sink (MCHS) on the idle side of the electronic component. The cooling fluid flows through the micro-scale channels, picking up the dissipated heat. The first microchannel heat sink was pioneered by Tuckerman and Pease in 1981 [1] and was considered a milestone in heat sink technology. Microchannel heat sinks have significantly lower thermal resistance than conventional heat sinks. Their effectiveness is explained by Newton's law of cooling and the definition of the Nusselt number as,

$$Nu = \frac{hd_H}{k_f} \tag{2-1}$$

In fully developed laminar flow, the Nusselt number is constant [2], and assuming constant fluid properties,

$$h \propto \frac{1}{d_H} \tag{2-2}$$

The smaller the channel's hydraulic diameter is, the more significant the heat transfer coefficient. Additionally, dividing the macro size channel into hundreds of microscale channels significantly increases the heat transfer area of the heat sink. Increased heat transfer coefficient and cooling surface are the main reasons that microchannel heat sinks are more effective thermally compared to regular heat sinks. However, some challenges

associated with MCHSs need to be addressed. One of the main challenges is the stream-wise temperature rise in MCHSs. As the liquid flows through the channel, it picks up the heat from the electronic component, and its temperature rises. Essentially, the boundary layer thickness increases, and as a result, the heat transfer coefficient is reduced in the streamwise direction. This phenomenon creates a temperature gradient on the cooling surface, leading to thermal stress and damage to electronic chips.

Another challenge is the decreased size of channels which increases the friction forces between the liquid and channel walls. The pressure drop in channels can be expressed as,

$$\Delta p = f\ \frac{l}{d_H}\ \frac{\rho u^2}{2} = 4\ C_f\ \frac{l}{d_H}\ \frac{\rho u^2}{2} = 2\ C_f\ Re\ \frac{l}{{d_H}^2}\ \mu\ u \tag{2-3}$$

For the fully developed laminar flow, the $C_f . Re$ term remains constant,

$$\Delta p \propto \frac{u}{{d_H}^2} \tag{2-4}$$

Thus, decreasing the diameter results in an increased pressure drop, another challenge associated with MCHSs.

Many studies have been performed to improve the thermal and hydraulic performance of MCHS. One of the most significant innovations in MCHS design is double-layer and multi-layer MCHSs, first established by Vafai and Zhu [3-5]. Vafai and Zhu [3] demonstrated that utilizing two layers of MCHS with counter flow configuration on top of each other decreases the stream-wise temperature rise dramatically compared to regular single-layer MCHS. It also offers a more uniform temperature distribution. Many other numerical and experimental studies have shown that double- and multi-layer MCHS designs have higher thermal capability than single-layer ones. Wei and Joshi [6]

investigated multi-layer MCHS with flexible control over each layer's flow direction and flow rate. This study indicates that multi-layer MCHSs are more efficient regarding pumping power requirements. Patterson et al. [7] numerically investigated the thermal performance of stacked microchannels with different flow arrangements. They reported that the counter flow arrangement proved to have the most uniform temperature distribution for the range of flow rates they studied. In contrast, the parallel flow configuration performs best in reducing the peak temperature. Similar results were reported by Wei et al. [8,9]. Levac et al. [10] investigated the effect of Reynolds number, inlet velocity profile, and flow configuration in the channels of the MCHS. They found that within the range $116 \leq Re \leq 1160$, the two-layer MCHS with counter flow has the lowest peak temperature, while the peak temperature in parallel flow arrangement is lower at Re <~ 100. Wong and Muezzin [11] also established that counter flow configuration is superior to parallel flow for high Reynolds numbers. Regarding the uniformity of temperature on the chip, the counter flow arrangement performed better than parallel flow at all values of Re. Lin et al. [12, 13] performed a thorough parametric investigation on double and multi-layer MCHS to better understand the design factors concerning channel dimensions, pumping power distribution, and flow configuration. They established that the optimized flow configuration is (0,1), (0,1,1), (0,1,1,1), respectively, for two-, three- and four-layer MCHSs ('0' stands for flow in positive x-direction and '1' stands for flow in negative x-direction). Their result shows that the counter flow arrangement is more effective when applied to the first two layers of channels. Lu and Vafai [14] thoroughly compared innovative MCHSs, including two-layer and multi-layer MCHS, showing that

double-layer and multi-layer MCHS have lower thermal resistance and temperature gradient, and require less pumping power.

This chapter focuses on optimizing MCHS designs for electronic cooling applications with constant heat flux at the base. MCHSs with rectangular and triangular cross-sections and counter flow arrangement in adjacent channels (Counter Dual MCHSs) are thoroughly investigated.

2.2. Approach and Methodologies

Two MCHS designs studied in this work utilize counter flow arrangement in adjacent channels, referred to as Counter Dual MCHSs in this work. The proposed Counter Dual MCHS geometries feature rectangular and triangular channel cross-sectional configurations, as depicted in Figure 2-3 and 2-4. To simulate the fluid flow and conjugate heat transfer in MCHSs, a three-dimensional model using the finite volume discretization method was developed with the COMSOL Multiphysics program. To reduce computational costs, the computational domain is selected by considering symmetry when investigating counter flow arrangement in the adjacent channels. The schematic view of the MCHSs and their corresponding computational domains are illustrated in Figures 2-1 to 2-4.

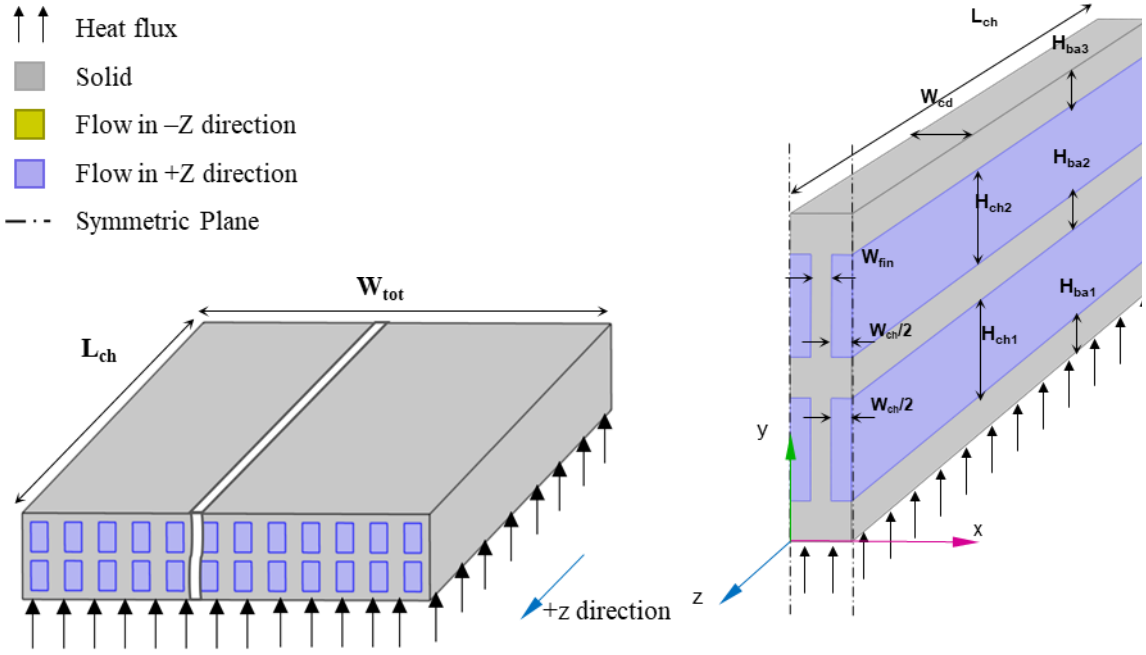

(a) Isometric view of the heat sink. **(b)** Computational Domain.

Figure 2-1 Schematic view of Double-Layer Parallel Flow MCHS.

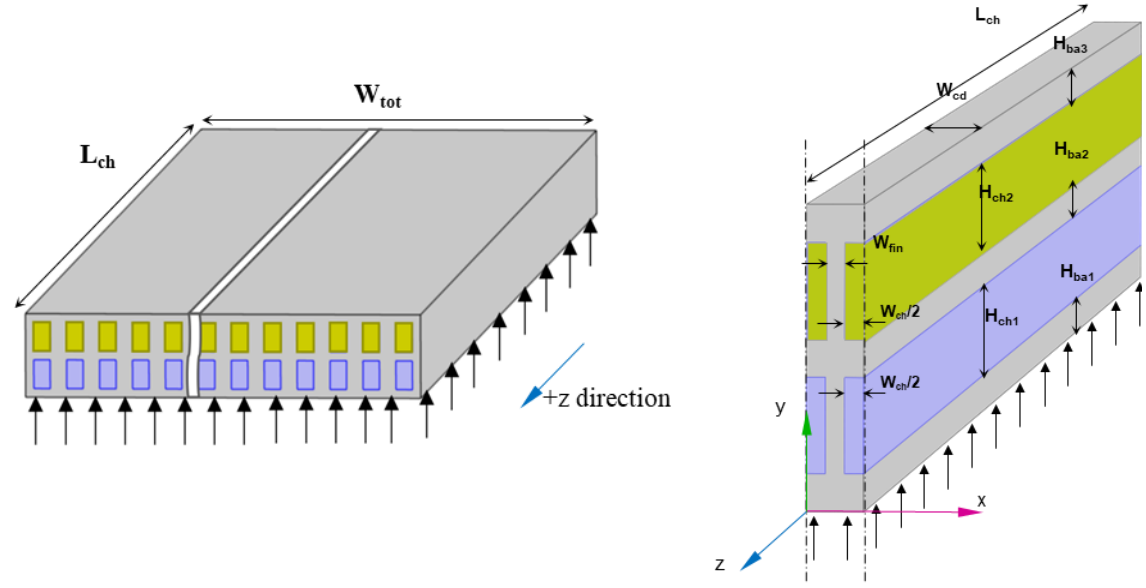

(a) Isometric view of the heat sink. **(b)** Computational Domain.

Figure 2-2 Schematic view of Double-Layer Counter flow MCHS introduced by Vafai and Zhu [3-5].

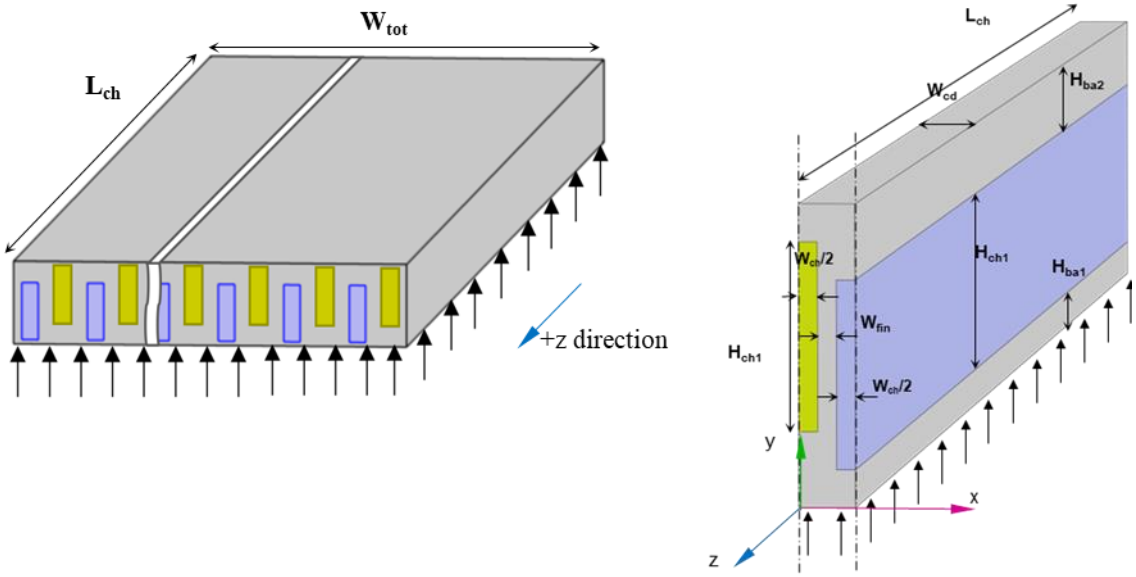

(a) Isometric view of the heat sink **(b)** Computational Domain

Figure 2-3 Schematic view of Counter Dual MCHS with rectangular cross-section.

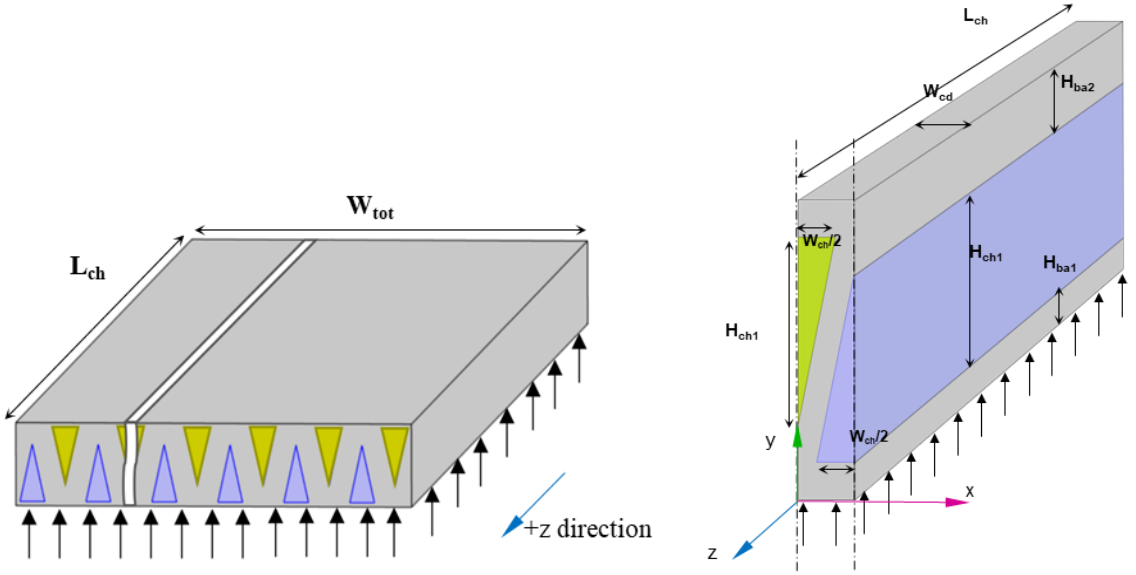

(a) Isometric view of the heat sink **(b)** Computational Domain

Figure 2-4 Schematic view of Counter Dual MCHS with triangular cross-section.

Based on previous studies [3, 15-20], this investigation makes several assumptions, including 1) steady-state condition, 2) incompressible and laminar flow, 3) negligible viscous dissipation and gravity effect, 4) constant thermophysical properties in the fluid and solid, 5) negligible entrance and exit effect at the inlet and outlet. The governing equations for the fluid region include the following.

Conservation of mass,

$$\nabla.\vec{V} = 0 \tag{2-5}$$

Conservation of momentum,

$$\rho_l(\vec{V}.\nabla)\vec{V} = -\nabla p + \mu_l\nabla^2\vec{V} \tag{2-6}$$

Conservation of energy,

$$\rho_l c_{p,l}(\vec{V}.\nabla)T_l = k_l\nabla^2 T_l \tag{2-7}$$

And the energy equation for the solid,

$$k_s\nabla^2 T_s = 0 \tag{2-8}$$

where $\vec{V}$, p, and T are the velocity vector, pressure, and temperature, respectively. Subscripts *l* refers to liquid, and *s* indicates solid properties.

Uniform heat flux is applied at the microchannel's bottom wall, accounting for the heat generated in the electronic substrate. To concentrate on the heat removal by the set-up, the upper wall of the heat sink is considered not to remove much heat and as such, heat is not dissipated from the top wall. The conductive heat from the solid walls at the inlet and outlet is neglected and concentrate on the heat removal from the device, the adiabatic boundary condition is applied to all external walls in the computational domain except for the bottom wall. At the inlet, a constant fluid temperature is assumed, while the adiabatic

condition is applied at the outlet. The atmospheric pressure condition is applied at the outlet, and a pressure boundary condition with no viscous stress is applied at the inlet to maintain a fixed pressure drop along the channel. However, for fixed flow rate cases, a fully developed velocity condition is used at the inlet. At all solid-liquid interfaces, no-slip boundary conditions and continuous temperature and heat flux are employed. These assumptions are consistent with previous analyses [3, 7, 15-20].

The thermal resistance is defined as

$$R_T = \frac{T_{max} - T_{min}}{q'' A} \tag{2-9}$$

where T_{max} represent the hottest temperature in the heat sink and T_{min} is the lowest temperature in the heat sink, which is the same as the coolant inlet temperature. A represent the cooling surface area and q'' is the applied heat flux at the base surface of the heat sink.

2.3. Model Validation

The 3D numerical model developed for MCHSs in this study is validated using experimental data from Wei et al. [21]. To ensure accuracy, grid-independence test is conducted by comparing results using three mesh sizes in a DLPF-MCHS. The fluid and solid temperature profiles estimated by the three mesh distributions at the symmetric line (d) are shown in Figure 2-5. Based on the results, the medium grid setting is adopted for this work.

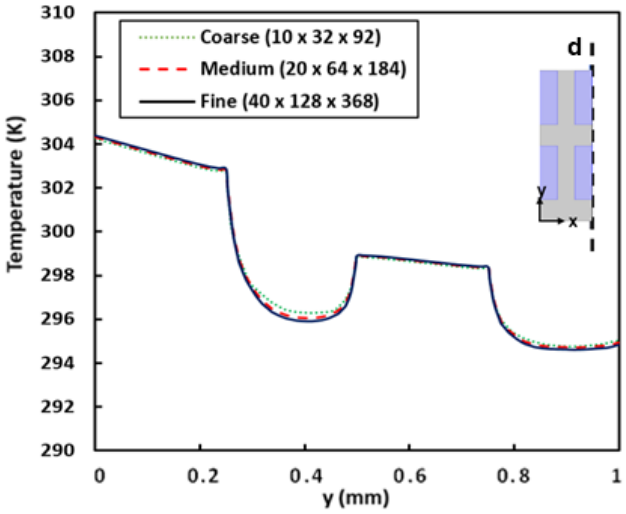

Figure 2-5 Grid independence study – MCHS model.

Wei et al. [21] conducted two sets of experiments for both parallel flow and counter flow arrangements at various flow rates. Figures 2-6 and 2-7 show the bottom wall temperature comparison for parallel and counter flow studies, respectively. The comparisons indicate excellent agreement between the MCHS simulation performed in this study and experimental data.

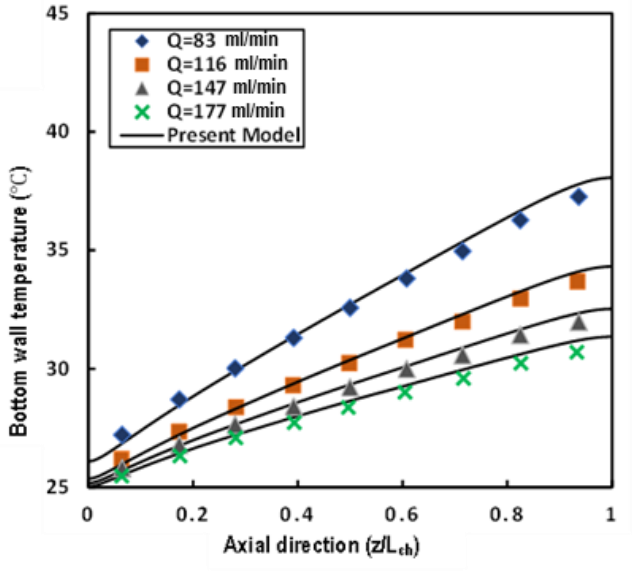

Figure 2-6 Validation with experimental data of Wei at al. [21] - Bottom wall temperature distribution for double layer parallel flow configuration MCHS.

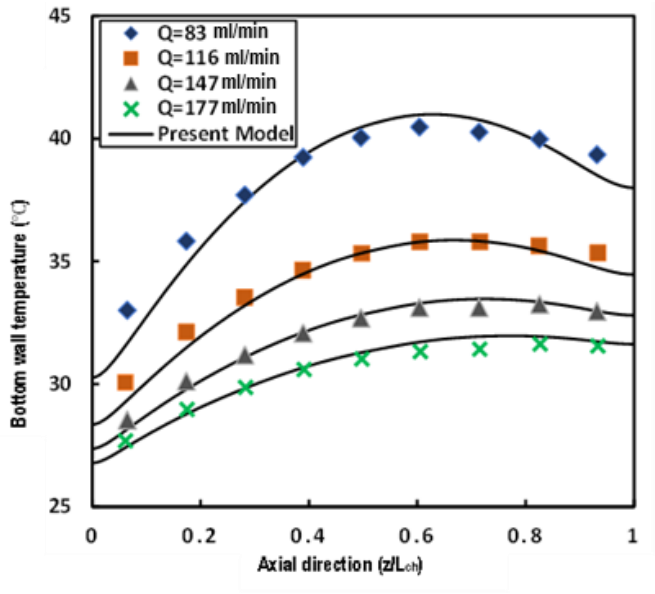

Figure 2-7 Validation with experimental data of Wei at al. [21] - Bottom wall temperature distribution for double layer counter flow configuration MCHS.

Table 2-1 Microchannel heat sink parameter specifications used in this work.

Specification	DLPF and DLCF MCHS	Counter Dual Rectangular MCHS	Counter Dual Triangular MCHS
Material (solid-Liquid)	Copper-Water	Copper-Water	Copper-Water
Total length of heat sink (L_{ch})	1 [cm]	1 [cm]	1 [cm]
Total width of heat sink (W_{tot})	1 [cm]	1 [cm]	1 [cm]
Computational domain width (W_{cd})	150 [μm]	150 [μm]	150 [μm]
First layer channel height (H_{ch1})	250 [μm]	500 [μm]	500 [μm]
Second layer channel height (H_{ch2})	250 [μm]	-	-
Channel width (W_{ch})	100 [μm]	100 [μm]	200 [μm]
Side wall thickness (W_{fin})	50 [μm]	50 [μm]	50 [μm]
Bottom wall thickness (H_{ba1})	100 [μm]	200 [μm]	200 [μm]
Middle wall thickness (H_{ba2})	100 [μm]	-	-
Top wall thickness (H_{ba3})	100 [μm]	100 [μm]	100 [μm]
Coolant Inlet Temperature	293.15 [K]	293.15 [K]	293.15 [K]
Heat flux at the base	100 [W/cm^2]	100 [W/cm^2]	100 [W/cm^2]

2.4. Results and Discussion

The performance of Counter Dual MCHSs with rectangular and triangular channel cross-sections is investigated and compared with DLPF and DLCF -MCHSs. The schematic of these heat sinks and the corresponding computational domains are illustrated in Figure 2-1 to 2-4, and the parameters used for this numerical analysis are listed in Table 2-1. The study is performed for both Silicon-Water and Copper-Water MCHSs, to investigate the impact of MCHS solid material.

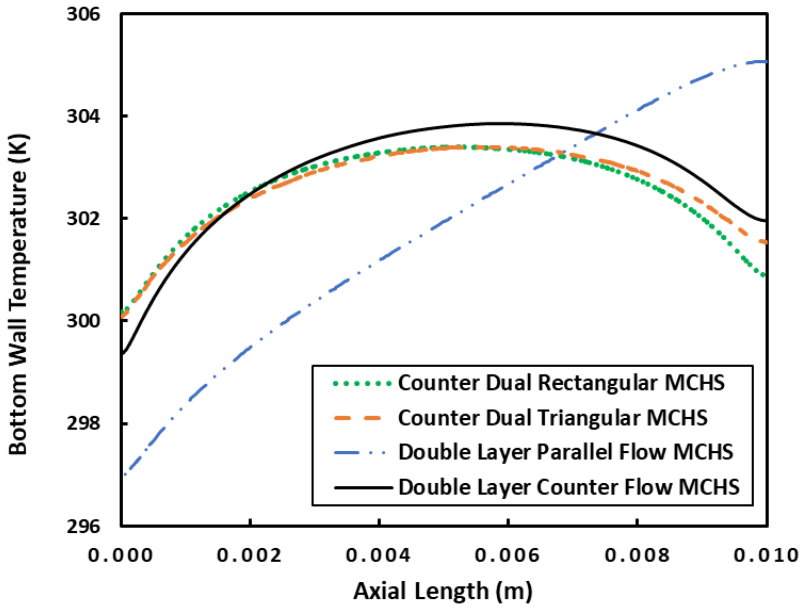

Figure 2-8 Bottom wall temperature in axial (z) direction of the studied Silicon-Water heat sinks at 0.05W pumping power.

The maximum temperature, surface temperature gradient, and thermal resistance of the studied MCHSs are compared in Figures 2-9 to 2-12 for Silicon-Water MCHSs, and the results for Copper-Water MCHSs are shown in Figures 2-13 to 2-16. The results show that the proposed configuration of Silicon-Water Counter Dual MCHS with rectangular cross-section reduces the surface temperature gradient of the heat sink by 43-50% and 26-

31% compared to DLPF and DLCF -MCHSs, respectively. The triangular cross-section also reduces it by 38-47% for parallel and 21-26% for counter flow arrangement, respectively. Additionally, the studied Counter Dual MCHSs reduce the thermal resistance of heat sinks by 10-15% compared to DLPF-MCHS and by 2-8% compared to DLCF-MCHS. A similar improvement trend is obtained for Copper-Water MCHSs.

The required pumping power, Reynolds number, and achieved flow rate are compared in Figure 2-17 and 2-18. The Counter Dual MCHSs with rectangular and triangular cross-sections lower pumping power by up to 15% and 30-40%, respectively, in the 50-400 ml/min flow rate range. They both deliver the highest Reynolds number as well.

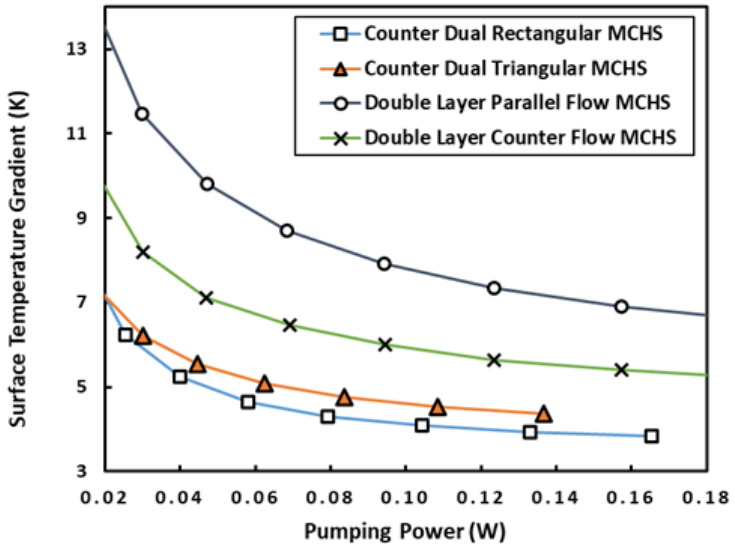

Figure 2-9 Comparison of the cooling surface temperature gradient of the studied heat sinks (Silicon-Water).

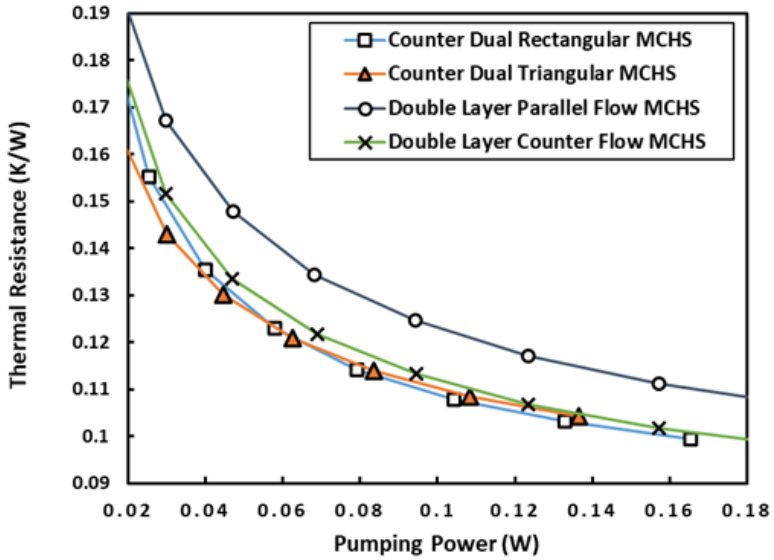

Figure 2-10 Comparison of the Thermal Resistance of the studied heat sinks (Silicon-Water).

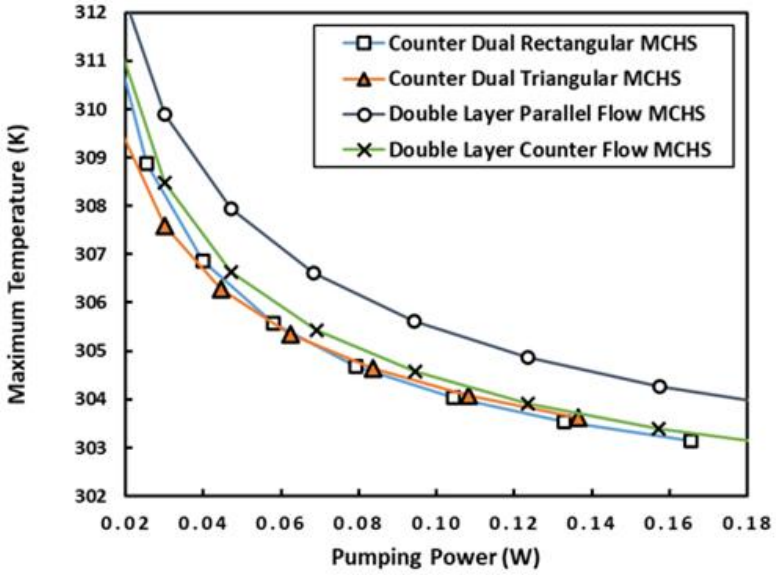

Figure 2-11 Comparison of the maximum temperature of the studied heat sinks versus pumping power (Silicon-Water).

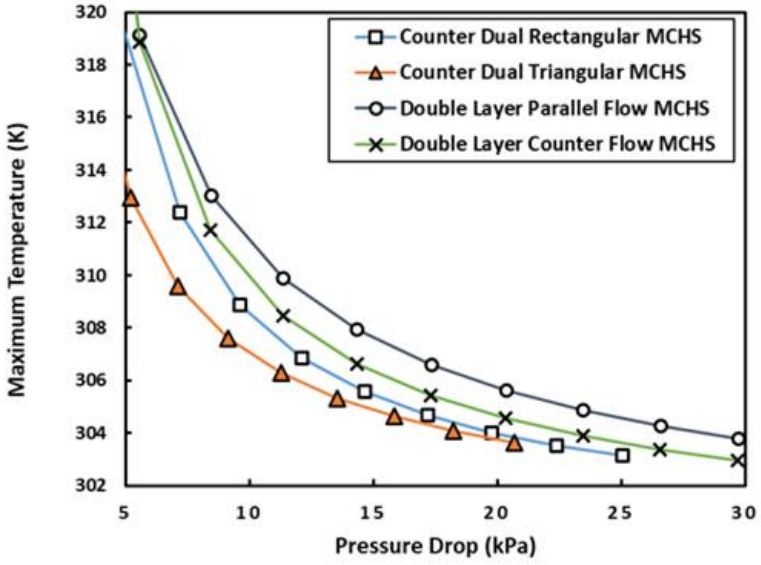

Figure 2-12 Comparison of the maximum temperature of the studied heat sinks versus pressure drop (Silicon-Water).

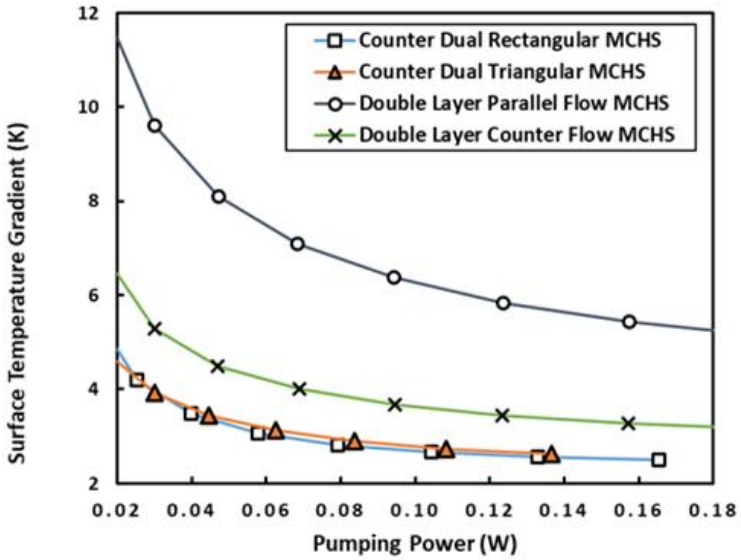

Figure 2-13 Comparison of the cooling surface temperature gradient of the studied heat sinks (Copper-Water).

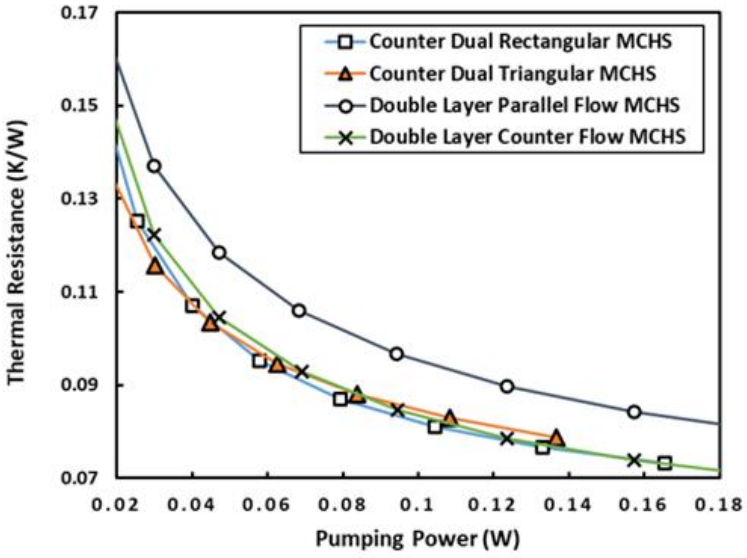

Figure 2-14 Comparison of the Thermal Resistance of the studied heat sinks (Copper-Water).

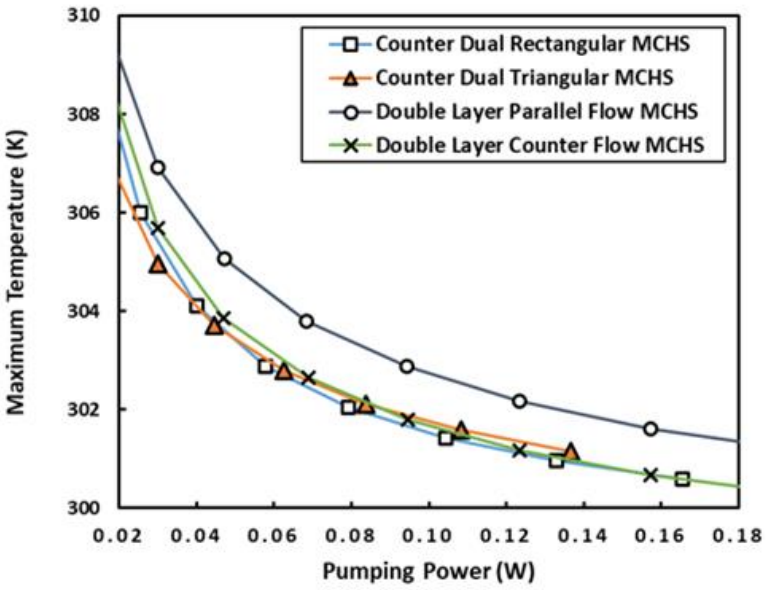

Figure 2-15 Comparison of the maximum temperature of the studied heat sinks versus pumping power (Copper-Water).

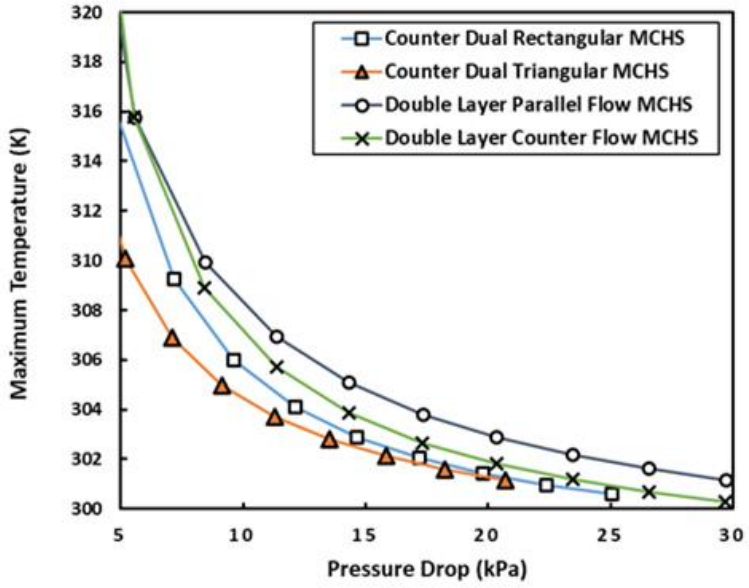

Figure 2-16 Comparison of the maximum temperature of the studied heat sinks versus pressure drop (Copper-Water).

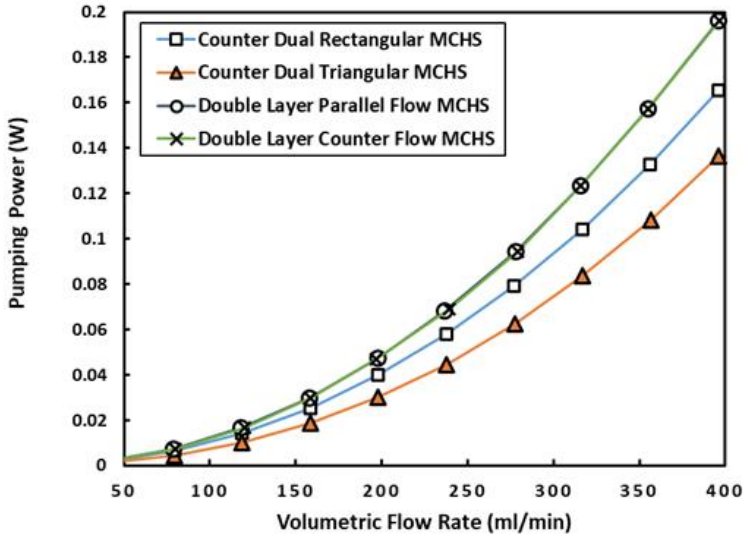

Figure 2-17 Comparison of the pumping power versus volumetric flow rate of the studied heat sinks (similar results for Silicon-Water and Copper-Water MCHSs).

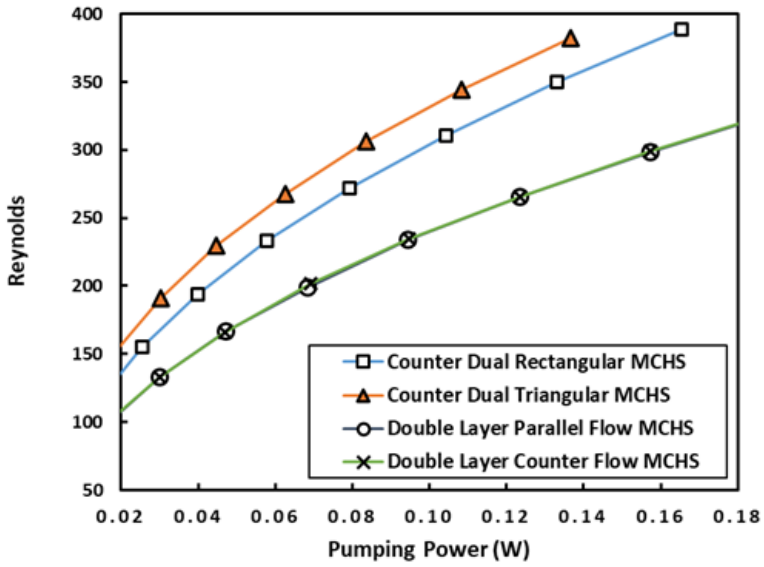

Figure 2-18 Comparison of the Reynolds number of the studied heat sinks (similar results for Silicon-Water and Copper-Water MCHSs).

The effect of the channel's aspect ratio on the thermal resistance of the triangular cross-section Counter Dual MCHS is also investigated, and results are provided in Figure 2-19. It is observed that the higher the aspect ratio of the channels, the lower the thermal resistance and maximum temperature of the MCHS. However, this trend stops at an aspect ratio of around 3, beyond which increasing the aspect ratio no longer impacts the thermal resistance. There is a consistent trend in the change of thermal resistance and surface temperature gradient of the Counter Dual Triangular MCHS as the pumping power is varied.

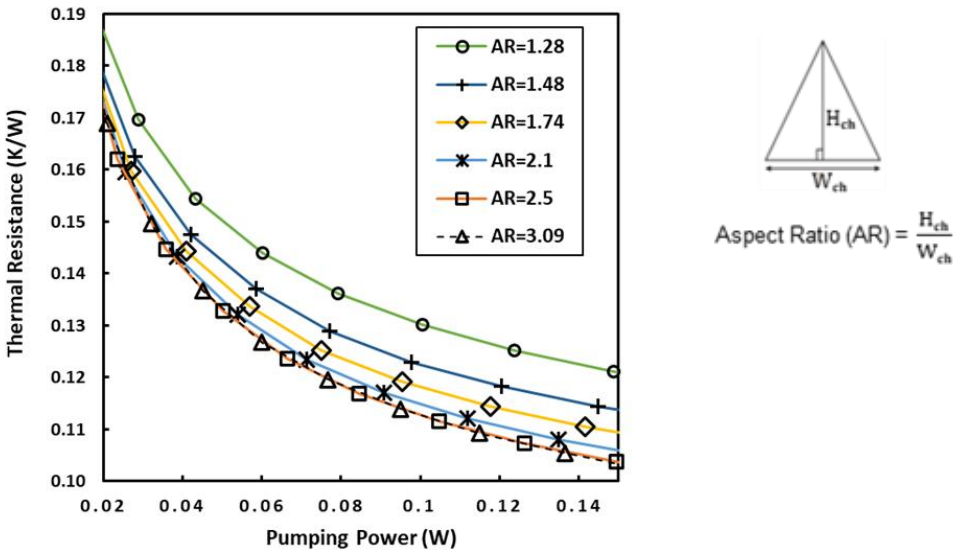

Figure 2-19 The impact of the aspect ratio of the channel on the thermal resistance of the Counter Dual Triangular MCHS at various pumping power (while keeping the channel cross-sectional area constant).

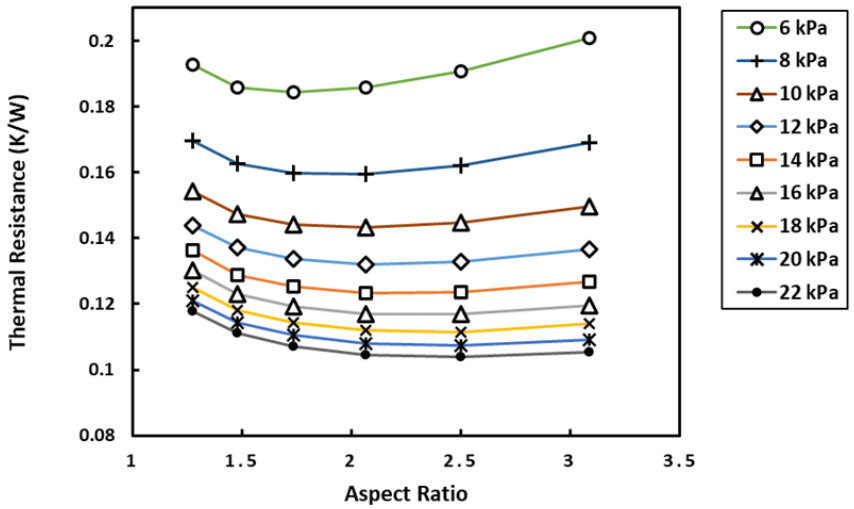

Figure 2-20 The impact of the aspect ratio of the channels and pressure drop on the thermal resistance of the Counter Dual Triangular MCHS (while keeping the channel cross-sectional area constant).

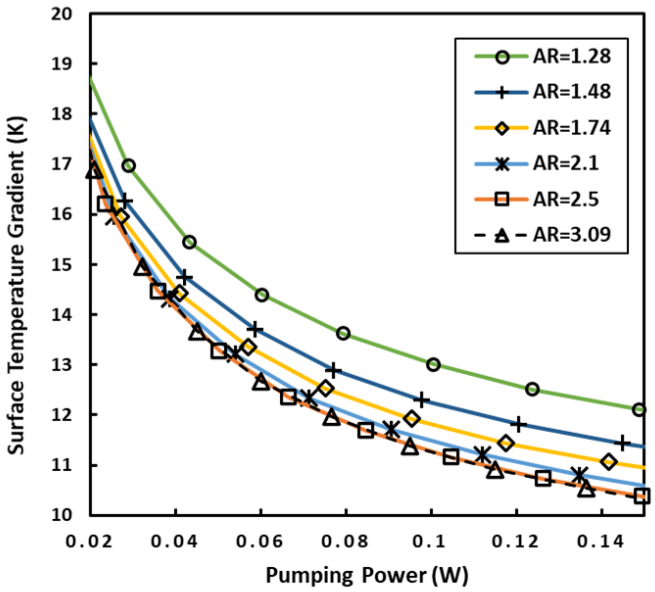

Figure 2-21 The impact of the aspect ratio of the channels on the surface temperature gradient of the Counter Dual Triangular MCHS (while keeping the channel cross-sectional area constant).

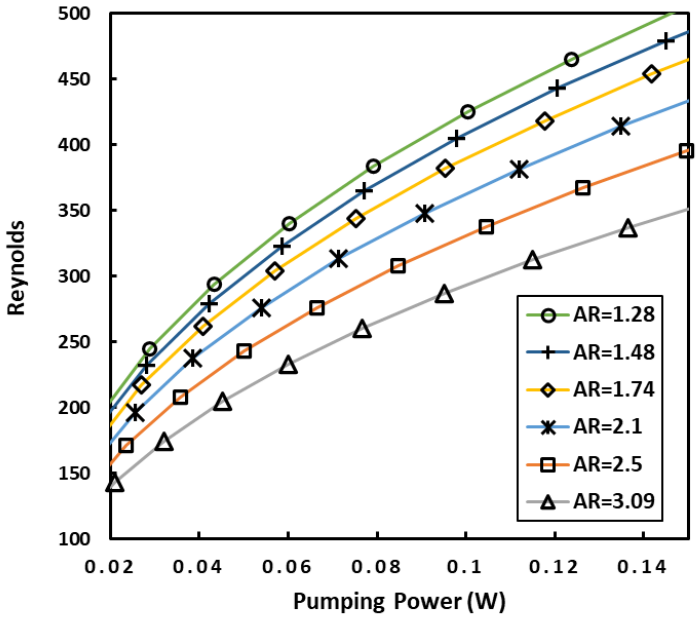

Figure 2-22 Reynolds number versus pumping power at various aspect ratio of the channels in Counter Dual Triangular MCHS (while keeping the channel cross-sectional area constant).

2.5. Conclusions

The performance of MCHSs with rectangular and triangular channel cross-sections and counter flow direction in adjacent channels are investigated and compared with double-layer MCHSs with parallel and counter flow arrangements. The study is performed for both Silicon-Water and Copper-Water MCHSs, to investigate the impact of MCHS solid material. The maximum temperature, surface temperature gradient, and thermal resistance of the studied MCHSs are compared. The main findings and conclusions are presented below.

- Through comparisons with experimental data, the reliability and accuracy of the three-dimensional finite volume method has been demonstrated within the scope of this study.

- The investigated configuration of Silicon-Water Counter Dual MCHS with rectangular cross-section reduces the surface temperature gradient of the heat sink by 43-50% and 26-31% compared to DL MCHSs with parallel and counter flow configuration, respectively. The triangular cross-section reduces it by 38-47% for parallel and 21-26% for counter flow arrangement, respectively.
- The studied Counter Dual MCHSs reduce the thermal resistance of heat sinks by 10-15% compared to DL-MCHS with parallel flow arrangement and by 2-8% compared to counter flow arrangement one.
- A similar improvement trend is obtained for Copper-Water MCHSs.
- The Counter Dual MCHSs with rectangular and triangular cross-sections require up to 15% and 30-40% lower pumping power, respectively, at 50-400 ml/min flow rates. They both deliver the highest Reynolds number as well.
- At a constant channel cross-sectional area, the higher the aspect ratio of the channels, the lower the thermal resistance and maximum temperature of the MCHS. However, this trend stops at an aspect ratio of around 3, beyond which increasing the aspect ratio no longer impacts the thermal resistance.
- As the pumping power is varied, the Counter Dual Triangular MCHS shows a consistent trend in the change of both its thermal resistance and surface temperature gradient.

References

[1] Tuckerman, D. B, Pease, R. F. W., “High-Performance Heat Sinking for VLSI”, Electron Device Letters, IEEE 2.5 (1981): 126 -129.

[2] Incropera, F. P., “Fundamental of Heat and Mass Transfer”, 8th edition, Wiley, New York (2007).

[3] Vafai, K., Zhu, L., “Analysis of two-layered micro-channel heat sink concept in electronic cooling”, International Journal of Heat and Mass Transfer (1999), 42: 2287-2297.

[4] Vafai, K., Zhu, L., “Two-layered micro-channel heat sink, devices and systems incorporating same”, U.S. Patent No. 6,457,515. 1 (2002).

[5] Vafai, K., Zhu, L., “Multi-layered micro-channel heat sink, devices and systems incorporating same”, U.S. Patent No. 6,675,875. 13 (2004).

[6] Wei, X., Joshi, Y., “Optimization study of stacked micro-channel heat sinks for micro-electronic cooling”, Components and Packaging Technologies, IEEE Transactions on 26.1 (2003): 55-61.

[7] Patterson, M. K., Wei, X., Joshi, Y., Prasher, R., “Numerical study of conjugate heat transfer in stacked microchannels”, Thermal and Thermomechanical Phenomena in Electronic Systems (2004), ITHERM'04. The Ninth Intersociety Conference on. IEEE.

[8] Wei, X., Joshi, Y., “Stacked microchannel heat sinks for liquid cooling of microelectronic components”, Journal of Electronic Packaging 126.1 (2004): 60-66.

[9] Wei, X., Joshi, Y., Patterson, M. K., “Stacked Microchannel Heat Sinks for Liquid Cooling of Microelectronics”, ASME International Mechanical Engineering Congress and Exposition. American Society of Mechanical Engineers (2004).

[10] Levac, M. L.-J., Soliman, H. M., Ormiston, S. J., “Three-dimensional analysis of fluid flow and heat transfer in single- and two-layered micro-channel heat sinks”, Heat and mass transfer 47.11 (2011): 1375-1383.

[11] Wong, K. C., Muezzin, F. N. A., “Heat transfer of a parallel flow two-layered microchannel heat sink”, International Communications in Heat and Mass Transfer (2013), 49: 136-140.

[12] Lin, L., Chen, Y.-Y., Zhang, X.-X., Wang, X.-D., “Optimization of geometry and flow rate distribution for double--layer microchannel heat sink”, International Journal of Thermal Sciences (2014), 78: 158-168.

[13] Lin, L., Deng, M.-X., Zhang, X.-X., Wang, X.-D., “Numerical analysis and parametric study of multilayered microchannel heat sinks”, Advances in Mechanical Engineering (2015), Vol. 7(7) 1–10.

[14] Lu, S., Vafai, K., “A comparative analysis of innovative microchannel heat sinks for electronic cooling”, International Communications in Heat and Mass Transfer (2016), 76: 271–284.

[15] Qu, W., Mudawar, I., Lee, S.-Y., Wereley, S. T., “Experimental and computational investigation of flow development and pressure drop in a rectangular micro-channel. J Electron Package (2006), 128:1–9.

[16] Fedorov, A. G., Viskanta, R., “Three-dimensional conjugate heat transfer in the microchannel heat sink for electronic packaging”, Int. J. Heat Mass Transfer (2000), 43: 399–415.

[17] Qu, W., Mudawar, I., “Analysis of three-dimensional heat transfer in micro-channel heat sinks”, Int. J. Heat Mass Transfer 45 (2002): 3973–3985.

[18] Tunc, G., Bayazitoglu, Y., Heat transfer in rectangular microchannels. Int. J. Heat Mass Transfer 45 (2002): 765–773.

[19] Kroeker, C. J., Soliman, H. M., Ormiston, S. J., Three-dimensional thermal analysis of heat sinks with circular cooling micro-channels. Int. J. Heat Mass Transfer (2004), 47: 4733–4744.

[20] Soliman, H. M., Rahman, M. M., “Analytical solution of conjugate heat transfer and optimum configurations of flat-plate heat exchangers with circular flow channels”, Heat Mass Transfer (2006), 42: 596–607.

[21] Wei, X., Joshi, Y., Patterson, M. K., “Experimental and numerical study of a stacked microchannel heat sink for liquid cooling of microelectronic devices”, Journal of Heat Transfer 129.10 (2007): 1432-1444.

Chapter 3: Hybrid Heat Sink designs combined with MCHS and Flat Plate Micro Heat Pipe.

3.1. Introduction

A heat pipe is a vacuum sealed metal tube with a thin wick layer on the internal surface. It contains a working fluid that circulates within the device and transfers heat from hot spots to cooler regions. When heat is introduced to a section of the heat pipe, called the evaporator section, the working fluid evaporates, and the hot vapor travels to the colder region, called the condenser section, where it condenses back to liquid. The capillary action forces the condensed liquid to travel back from the condenser to the evaporator section through the wick's porous structure [1]. The phase change allows the heat pipe to provide efficient and uniform cooling across large surfaces without needing external power input or moving parts. Heat pipe transfer heat much more efficiently than solid metal with a significantly lighter weight. They can also be combined with other cooling methods for additional thermal management. Traditional heat pipes are limited by their round shape, which makes it challenging to provide an effective cooling surface on smaller heat sources. Multi-channel Flat shaped heat pipes, established and investigated by Vafai et al. [2–6], overcome these limitations by providing better geometric adaptability and the ability to operate reliably under asymmetrical heat load conditions.

Most previous MCHS studies have relied on the assumption of a constant heat flux at the base area, which meant to represent a uniform heat generation by the chip. The

applications with local high heat flux, which can exceed ten times the average heat flux generated by the electronic substrate, are mostly overlooked.

In this chapter, innovative combined Heat Sink designs that utilize MCHS and Flat Plate Micro Heat Pipe (FPM-HP) are introduced. These hybrid designs are particularly beneficial for managing hotspots in electronic cooling applications that involve local high heat generation. Combining MCHS and HP technologies can achieve optimal cooling performance and ensure that the electronic device operates efficiently

3.2. Approach and Methodologies

Innovative hybrid heat sink designs combined with FPM-HP and MCHSs are investigated to optimize hotspot management in electronics cooling. The schematic of the studied hybrid heat sink designs with their corresponding computational domains are depicted in Figures 3-1 to 3-6. The governing equations and assumptions used for the MCHS section of these heat sinks are consistent with our previous study in section 2.1. The following are governing equations and assumptions used at various regions of the heat pipe.

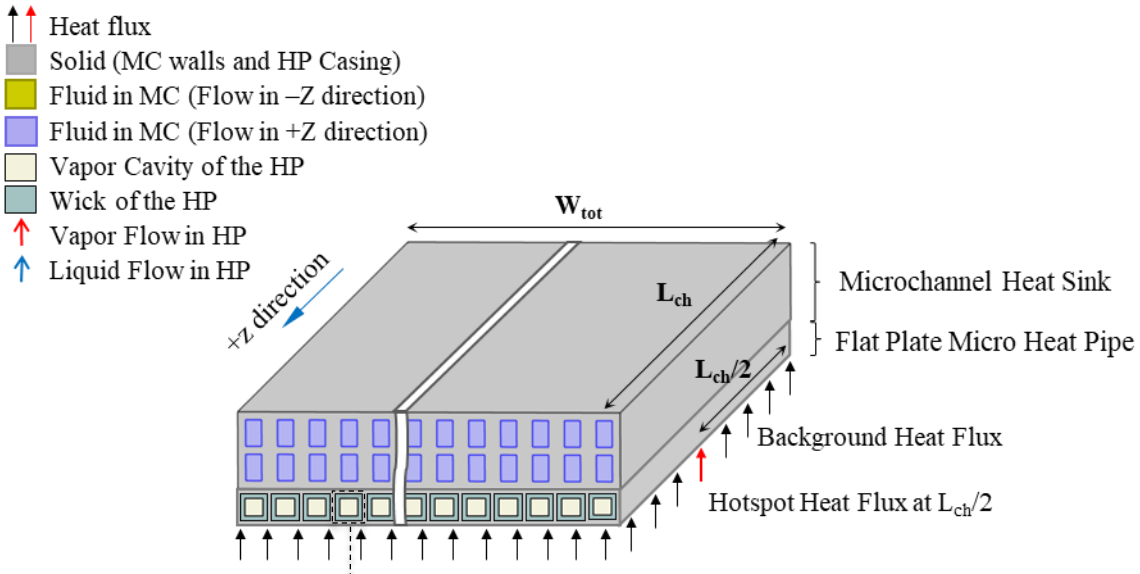

Figure 3-1 Schematic of Hybrid Heat Sink design combined with Double-Layer MCHS and Flat Plate Micro Heat Pipe studied in this work. (Isometric view)

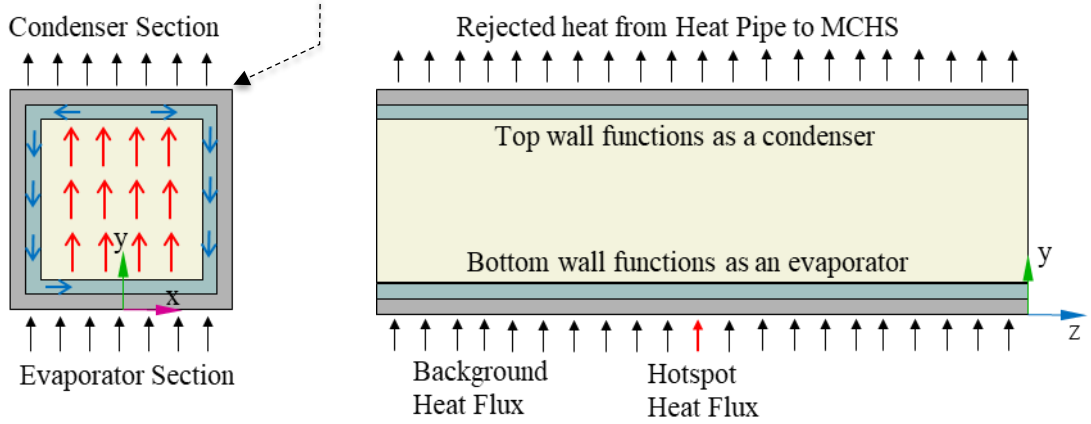

(a) **(b)**

Figure 3-2 Schematic of the heat pipe section as part of the Hybrid Heat Sink designs studied in this work. (a) Vertical cross sections, (b) Axial cross section.

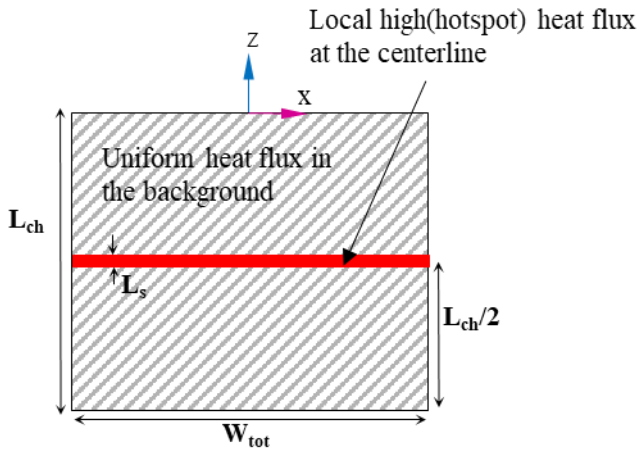

Figure 3-3 Bottom view of the Hybrid Heat Sink.

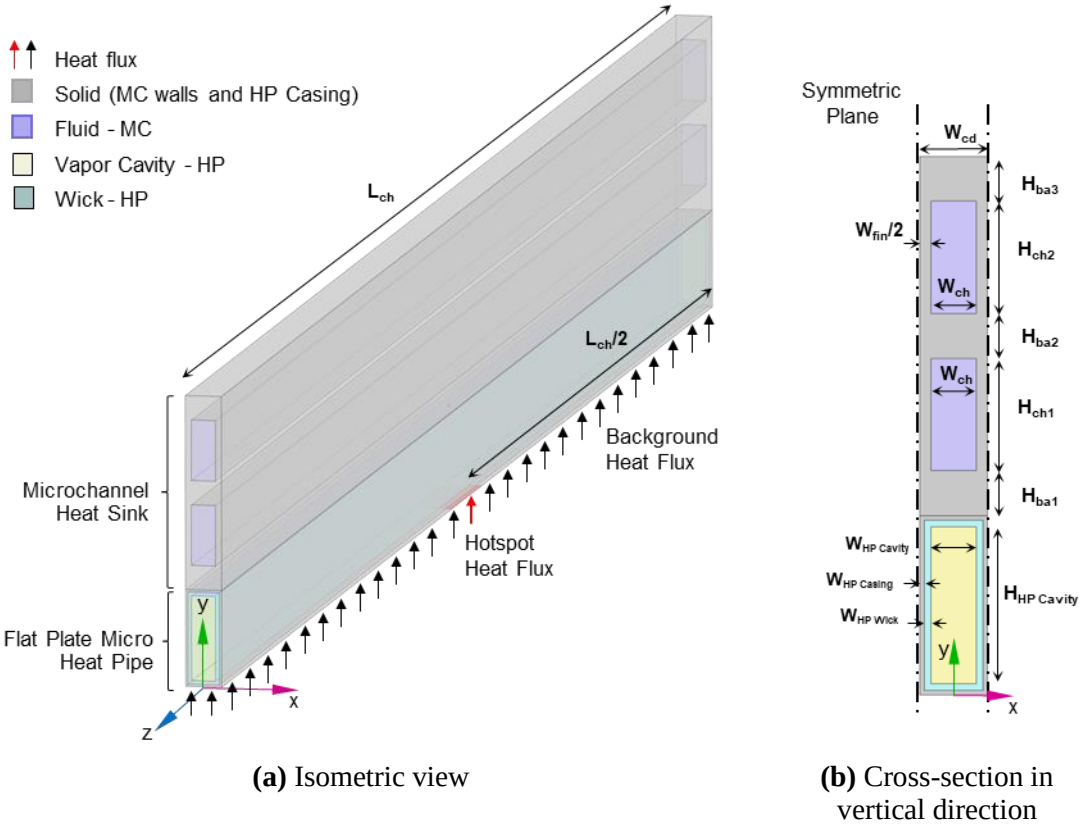

(a) Isometric view

(b) Cross-section in vertical direction

Figure 3-4 Computation domain used for analysis of the Hybrid DL MCHS & FPM-HP studied in this work

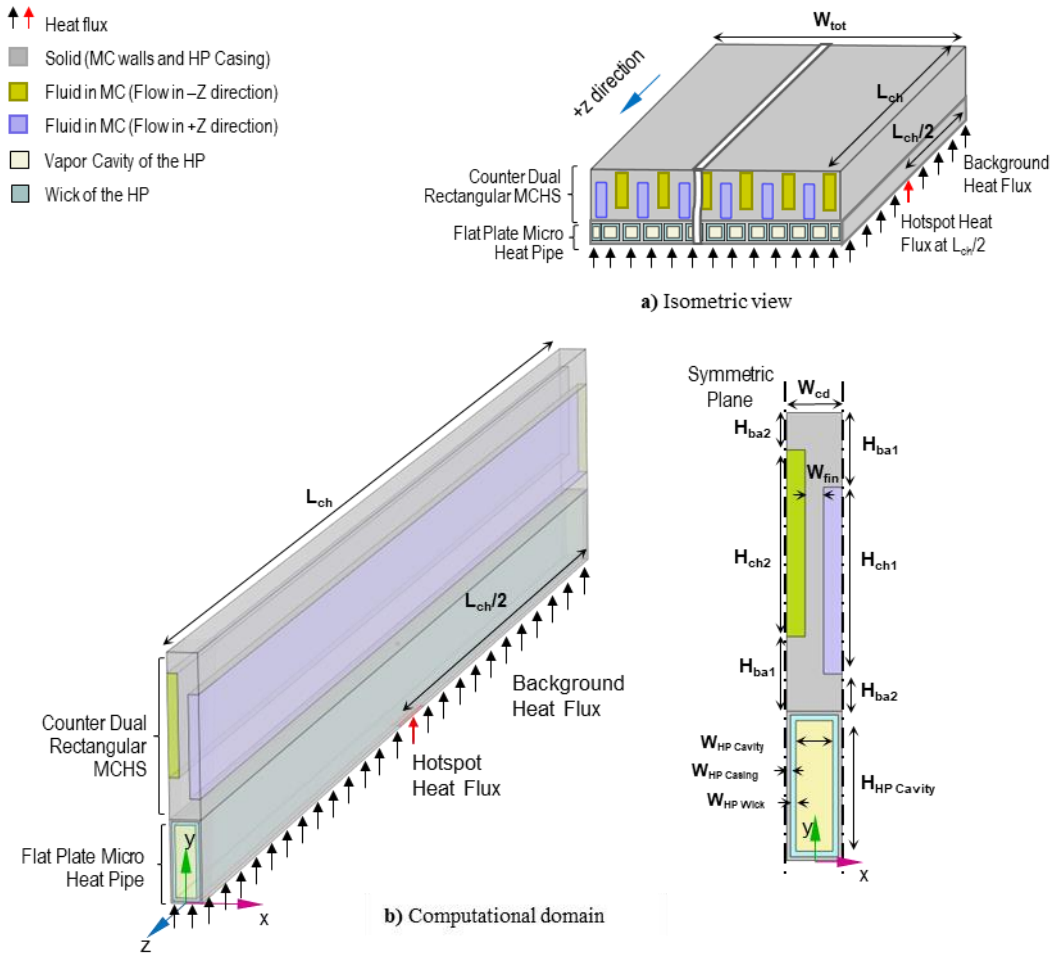

Figure 3-5 Schematic of the hybrid heat sink design combined with Counter Dual Rectangular MCHS and FPM-HP studied in this work.

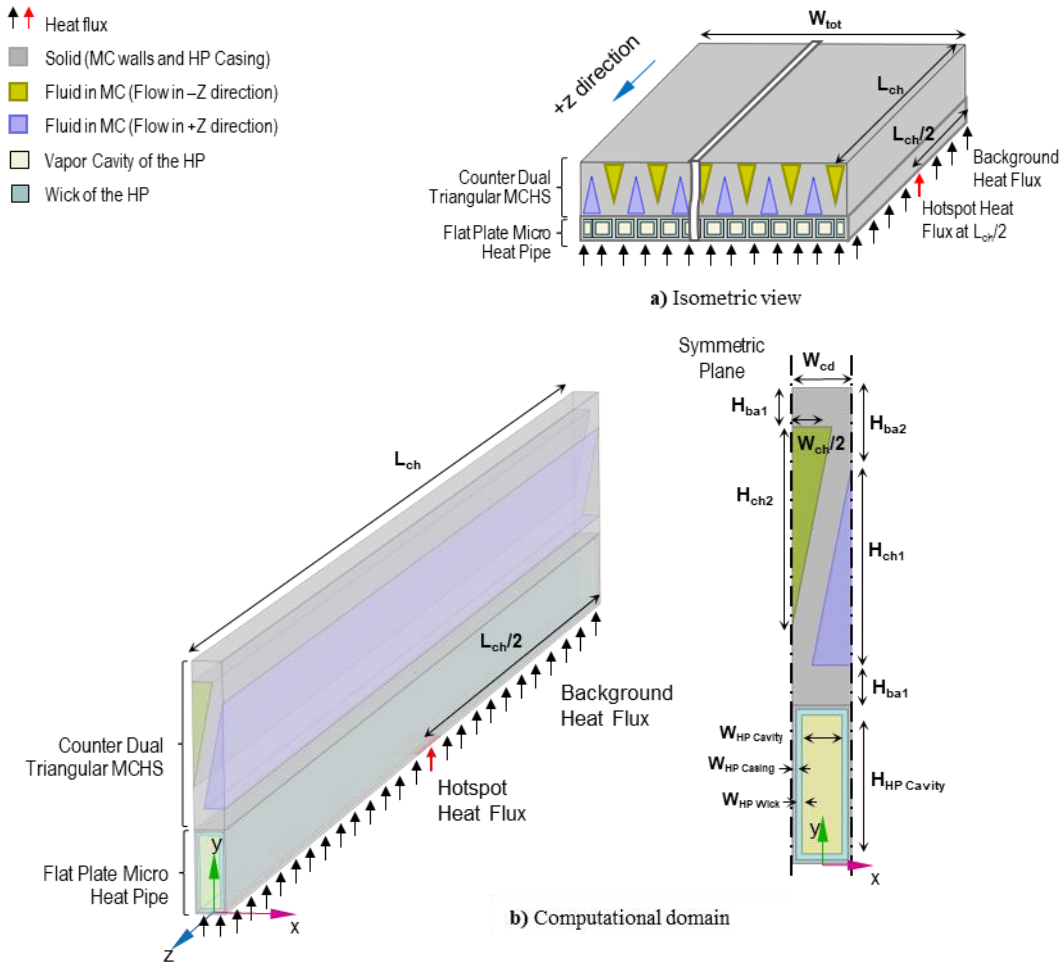

Figure 3-6 Schematic of the hybrid heat sink design combined with Counter Dual Triangular MCHS and FPM-HP studied in this work.

Cavity (vapor) region:

The assumptions made for the Cavity (vapor) region include 1) steady-state condition, 2) compressible and laminar flow, 3) negligible viscous dissipation and gravity effect, 4) constant thermo-physical properties.

Conservation of mass,

$$\nabla . \overrightarrow{V_v} = 0 \tag{3-1}$$

Conservation of momentum,

$$\rho_v \left(\overrightarrow{V_v} . \nabla\right) \overrightarrow{V_v} = -\nabla p_v + \mu_v \nabla^2 \overrightarrow{V_v} \tag{3-2}$$

Conservation of energy,

$$\rho_v c_{p,v} \left(\overrightarrow{V_v} . \nabla\right) T_v = k_v \nabla^2 T_v \tag{3-3}$$

Cavity-wick interface:

The coupled boundary condition is applied, and Water (in the wick) and vapor (in the cavity) are assumed at equilibrium.

$$p_v = p_{H_2O,sat}(T) \tag{3-4}$$

Boundary continuity and boundary heat flux is introduced at the Water (in wick) and vapor (in cavity) interface to introduce phase change.

$$\rho_l \overrightarrow{V_l} = \rho_v \overrightarrow{V_v} \tag{3-5}$$

$$Q = \dot{m}_v h_{fg}(T) \tag{3-6}$$

Wick (porous) region:

The assumptions made for the wick region include 1) no dry-out condition (wick is saturated with liquid), 2) the capillary pressure is enough to force the condensate back to the evaporator region, 3) steady-state condition, 4) compressible flow, 5) negligible inertial term and gravity effect, 6) constant thermo-physical properties.

Conservation of mass,

$$\nabla . \overrightarrow{V_l} = 0 \tag{3-7}$$

Conservation of momentum, according to Vafai and Tien [7],

$$0 = -\nabla \mathrm{p}_l + \mu_l \nabla^2 \overrightarrow{V_l} - \mu_l \frac{\epsilon}{K} \overrightarrow{V_l} \tag{3-8}$$

Conservation of energy (Liquid),

$$\rho_l \mathrm{c}_{p,l} \left(\overrightarrow{V_l} . \nabla \right) \mathrm{T}_l = \mathrm{k}_{eff} \nabla^2 \mathrm{T}_l \tag{3-9}$$

Solid Casing Region

Conservation of energy,

$$0 = \mathrm{k}_s \nabla^2 \mathrm{T}_s \tag{3-10}$$

3.3 Model Validation

The 3D numerical model of the heat pipe in this study is validated using experimental data from Huang et al. [8]. Grid-independence test is conducted by generating results at three grid sizes. Based on the results presented in Figure 8, the fine grid setting is adopted for this work. To further validate the model, the simulation results were compared with experimental data reported by Huang et al. [8], analytical results from Zhu and Vafai [9], and numerical results from Sanhan et al. [10]. Figure 9 (a) and 9 (b) show the heat pipe wall and vapor temperature comparison. The comparisons confirm remarkable consistency between the Heat Pipe simulation performed in this study and the cited validation data.

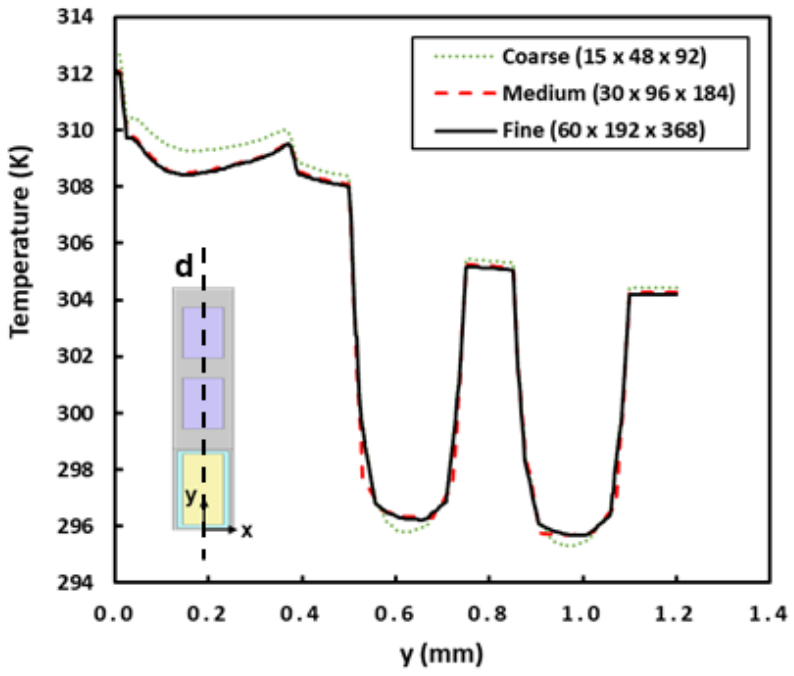

Figure 3-7 Grid independence study – Heat pipe model

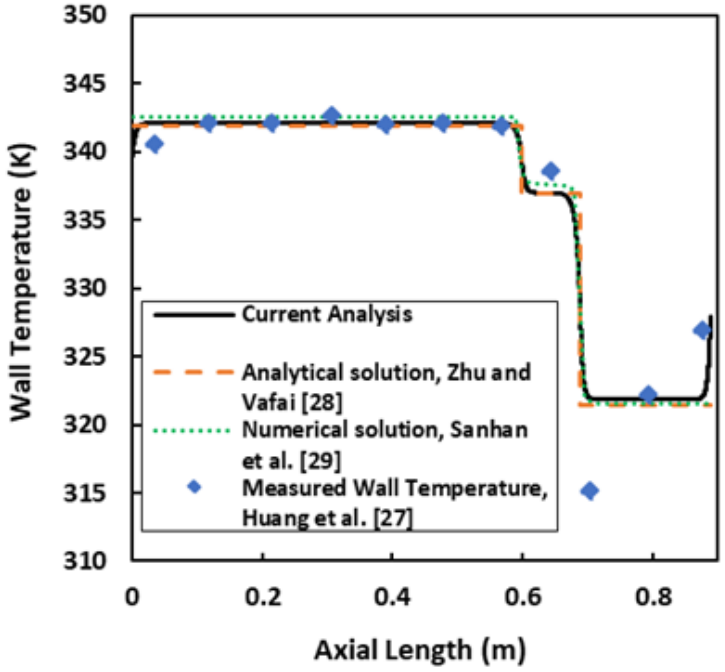

(a)

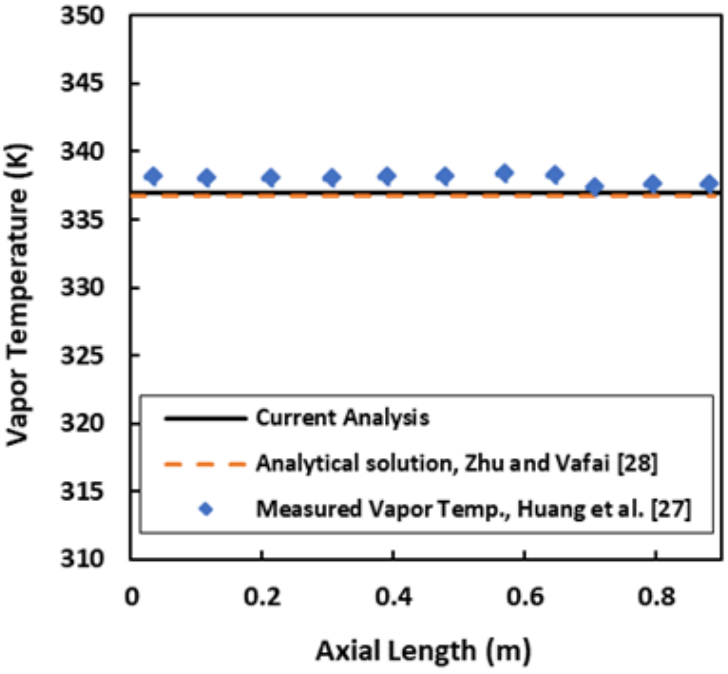

Figure 3-8 Comparison of the model results with pertinent numerical and experimental data in the literature. (a) Wall temperature, (b) Vapor temperature.

3.4 Result and Discussion

Innovative hybrid heat sink designs have been developed to optimize thermal and hot spot management in electronic cooling applications with local high heat generation at the base. These designs combine MCHS and FPM-HP technologies. The FPM-HP is inserted between the heat source and the MCHS bottom, to distribute the local high heat flux generated at the base. Figure 3-1 shows the schematic view of the hybrid heat sink combined with DL MCHS and FPM-HP. The proposed hybrid heat sinks combined with Counter Dual MCHS and FMP-HP are also provided in Figure 3-5 and 3-6 for rectangular and triangular cross-sections, respectively. The DL MCHS is investigated at both parallel and counter flow configurations. The studied cases include cooling of electronic substrate that generates 100 W/cm2 as background heat flux and high local heat flux of 600-1000 W/cm2 at the centerline of the base. The performance of the hybrid heat sink is compared with DL-MCHSs with a copper heat spreader at the base and with no heat spreader at all (short base). The schematic of the computational domains used for the hybrid heat sinks in this study are presented in Figures 3-4 to 3-6. Table 3-1 lists the parameters used for this numerical analysis.

Table 3-1 Heat pipe parameter specifications used in this work.

Specification	Value
Material (solid–Liquid)	Copper-Water
Total length of heat sink (L_{ch})	1 [cm]
Total width of heat sink (W_{tot})	1 [cm]
Casing thickness (W_{casing})	10 [μm]
Cavity width (W_{cavity})	100 [μm]
Wick layer thickness (W_{wick})	100 [μm]
Wick porosity (ε)	0.9
Wick permeability (K)	1.5e-9 [m^2]
Background heat flux at the base	100 [W/cm^2]
Hotspot heat flux at the base centerline	600 or 1000 [W/cm^2]
Width of hotspot heat flux (L_s)	600 [μm]

Figure 3-9 displays the temperature distributions of the studied heat sinks in axial cross section at 0.05W pumping power. The maximum temperature and surface temperature gradient of the heat sinks at various pumping powers are compared in Figure 3-10. The results show that hybrid heat pipe and microchannel heat sink investigated in this study has the lowest maximum temperature and surface temperature gradient among all the investigated designs in this study. The hybrid heat sink with parallel flow configuration design has the lowest maximum temperature, and the counter flow configuration one has the lowest surface temperature gradient compared to the rest of the studied heat sinks. In parallel flow configuration, the coolant temperature is lower at the center of the heat sink where the hot spot of the heat sink is located. This results in higher temperature difference between the coolant and the base at the hotspot, and therefore an improved thermal performance, compared to counter flow configuration ones.

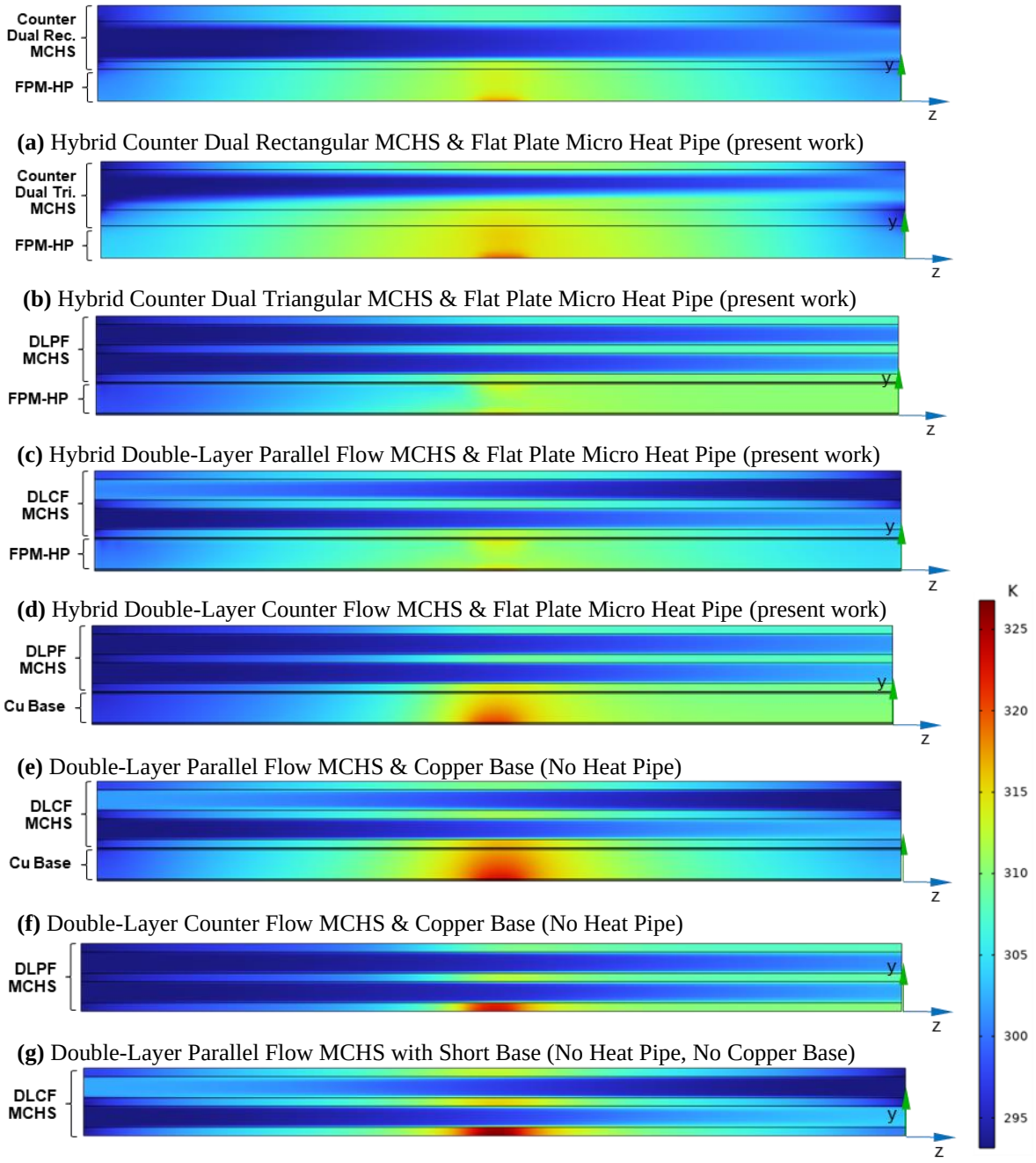

(a) Hybrid Counter Dual Rectangular MCHS & Flat Plate Micro Heat Pipe (present work)

(b) Hybrid Counter Dual Triangular MCHS & Flat Plate Micro Heat Pipe (present work)

(c) Hybrid Double-Layer Parallel Flow MCHS & Flat Plate Micro Heat Pipe (present work)

(d) Hybrid Double-Layer Counter Flow MCHS & Flat Plate Micro Heat Pipe (present work)

(e) Double-Layer Parallel Flow MCHS & Copper Base (No Heat Pipe)

(f) Double-Layer Counter Flow MCHS & Copper Base (No Heat Pipe)

(g) Double-Layer Parallel Flow MCHS with Short Base (No Heat Pipe, No Copper Base)

(h) Double-Layer Counter Flow MCHS with Short Base (No Heat Pipe, No Copper Base)

Figure 3-9 Temperature distribution of the heat sink in axial cross section at x = 0 (Hotspot heat flux at centerline: 1000 W/cm^2, Background heat flux: 100 W/cm^2)

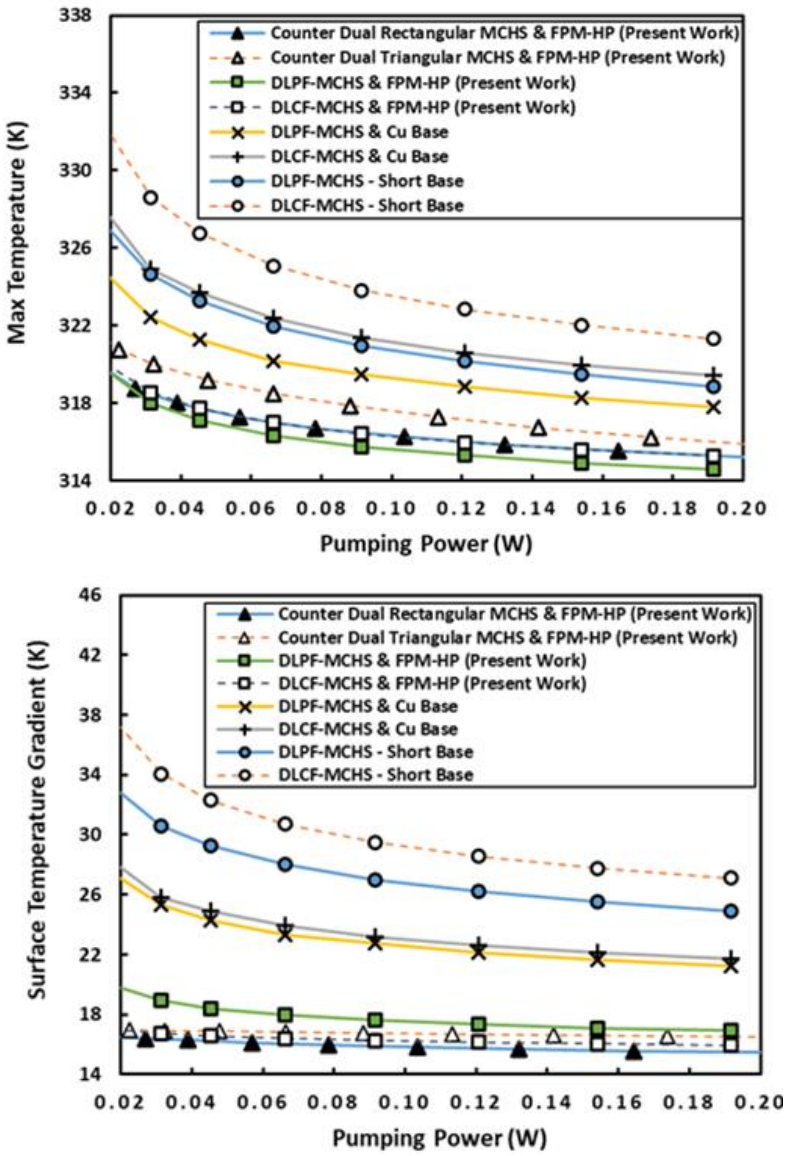

Figure 3-10 Comparison of the maximum temperature and the cooling surface temperature gradient of the studied hybrid heat sinks (Hotspot heat flux at centerline: 1000 W/cm^2, Background heat flux: 100 W/cm^2).

The hybrid DLPF-MCHS combined with FPM-HP reduces the maximum temperature and surface temperature gradient of the heat sink by 13-23% and 20-49%, and the counter flow one reduces them by 16-40% and 27-64% compared to copper base (no heat pipe) design, respectively. The hybrid Counter Dual Rectangular MCHS & FPM-HP reduces the maximum temperature and surface temperature gradient of the heat sink by 15-24% and 29-65%, while these are reduced by 10-26% and 24-63% for the Counter Dual Triangular MCHS, respectively, compared with the DLCF MCHS with copper base (no heat pipe) design.

The velocity field of the vapor and liquid in the heat pipe section of the studied hybrid heat sinks with Counter Dual Rectangular and Triangular MCHSs, and with DLPF MCHSs are shown in Figures 3-11, 3-12, and 3-13, respectively. The results show that the vapor and liquid velocity filed in the heat pipes attached to the counter flow MCHSs are similar in trend and magnitude. In all hybrid heat sinks, the heat pipe's bottom surface acts as an evaporator, and its top surface acts as a condenser section. The water evaporates at the bottom of the heat pipe where it is in contact with the heat source. The vapor then travels to the top surface of the heat pipe, where the microchannel heat sink cools it down and condenses it back to liquid. The capillary action forces the condensed liquid to travel back to the evaporator section (bottom surface) through the porous structure of the wick. The velocity profile in the vertical and axial cross-section of the heat pipe shows that two sets of coolant circulating loops occur mainly in the heat pipes in this study. The primary circulating loops occur in the vertical cross-sections (xy planes) by vapor and liquid circulating from the bottom to top surface of the heat pipe and return in fixed z height

planes, as shown in Figures 3-11 to 3-12 (c), (d), and (e). The local high heat source at the center of the heat pipe base imposes secondary circulating loops of the water which occur from the bottom center of the heat pipe to the top right and top left side of the heat pipe, as shown in Figure 3-11 to 3-12 (a) and (b). The secondary coolant circulating loop to one side of the heat pipe is more significant than the other, due to the asymmetric nature of the cooling in the MCHS, with coolant temperature rising in the flow direction. This difference is more significant in the parallel flow MCHS which is much colder close to the inlet side than the counter flow arrangement. This result emphasizes the capability of the heat pipes to operate well in asymmetrical heating and cooling load conditions.

The comparison analysis is repeated with the case of 600 W/cm^2 hotspot heat flux while the background heat flux remains constant at 100 W/cm^2. The trend of improvements remains consistent for both 600 and 1000 W/cm^2 cases of hotspot heat flux.

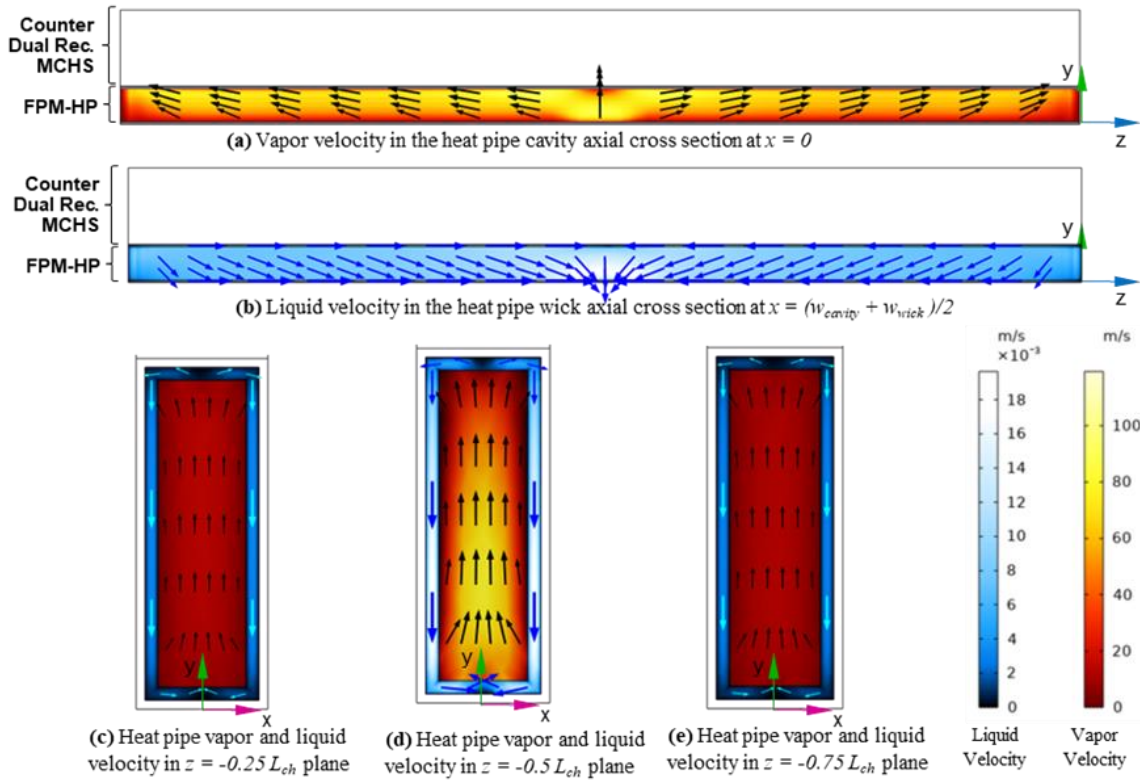

Figure 3-11 Velocity field in the heat pipe as part of the hybrid Counter Dual Rectangular MCHS & Flat Plate Micro Heat Pipe heat sink (Hotspot heat flux at centerline: 1000 W/cm^2, Background heat flux: 100 W/cm^2).

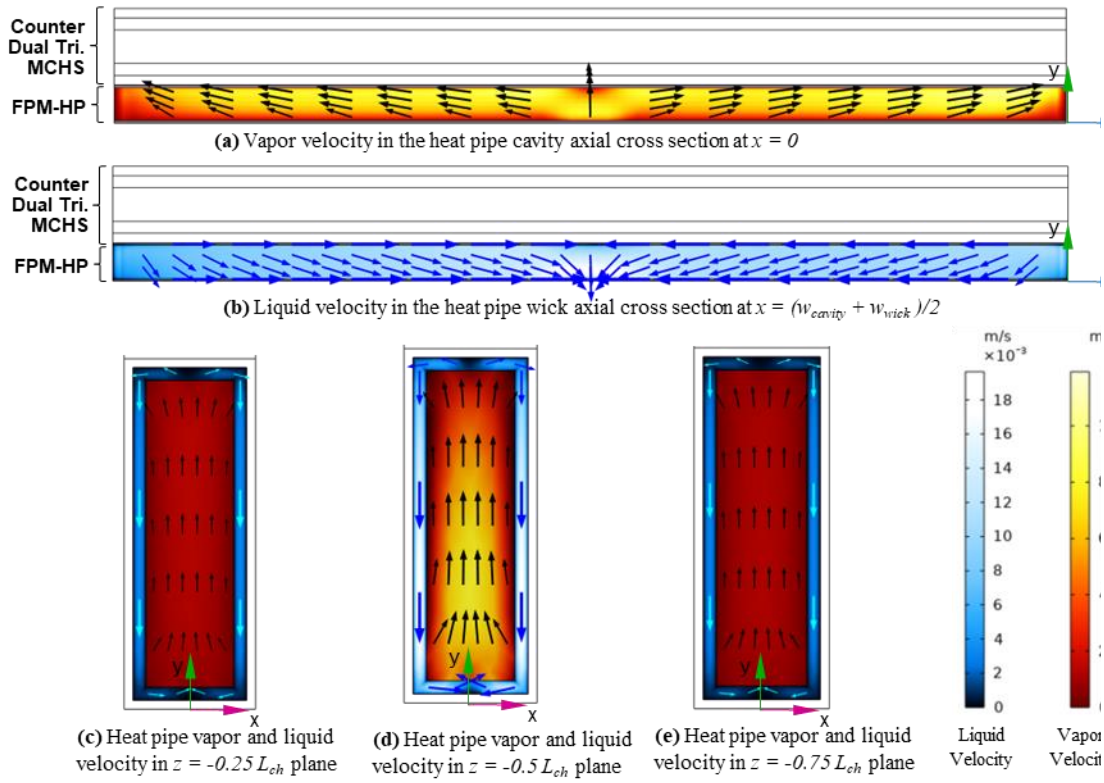

Figure 3-12 Velocity field in the heat pipe as part of the hybrid Counter Dual Triangular MCHS & Flat Plate Micro Heat Pipe heat sink (Hotspot heat flux at centerline: 1000 W/cm^2, Background heat flux: 100 W/cm^2).

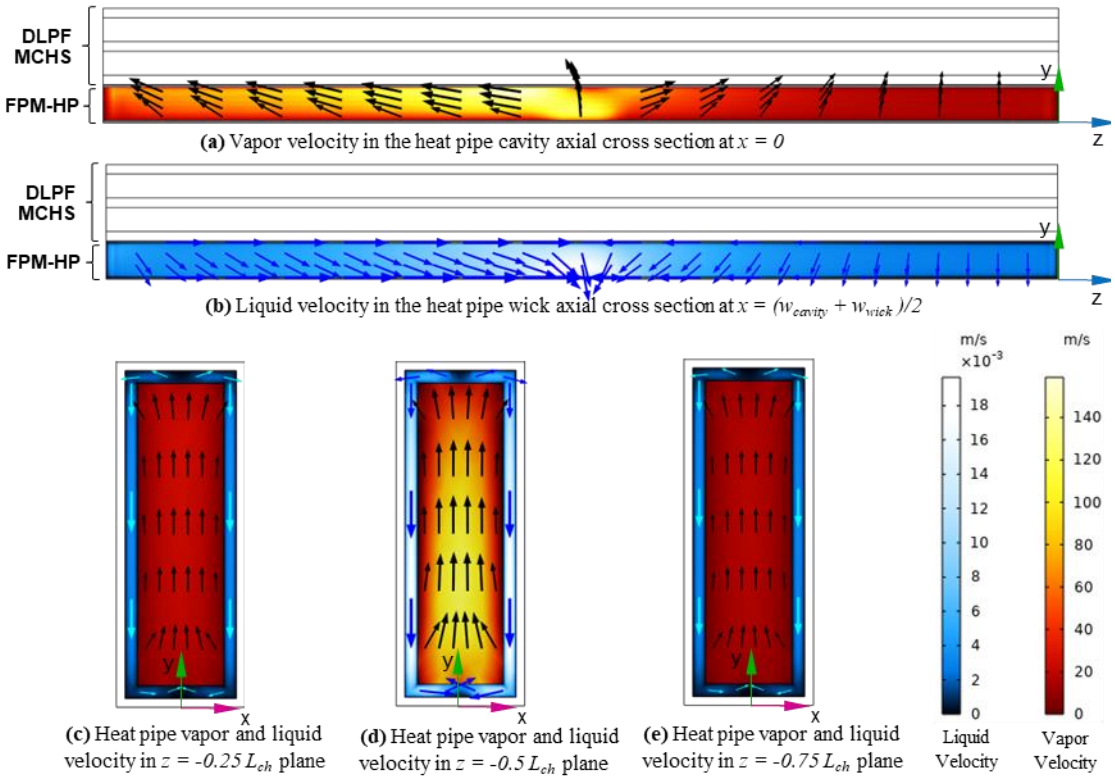

Figure 3-13 Velocity field in the heat pipe as part of the hybrid Double-Layer Parallel Flow MCHS & Micro Heat Pipe heat sink (Hotspot heat flux at centerline: 1000 W/cm^2, Background heat flux: 100 W/cm^2).

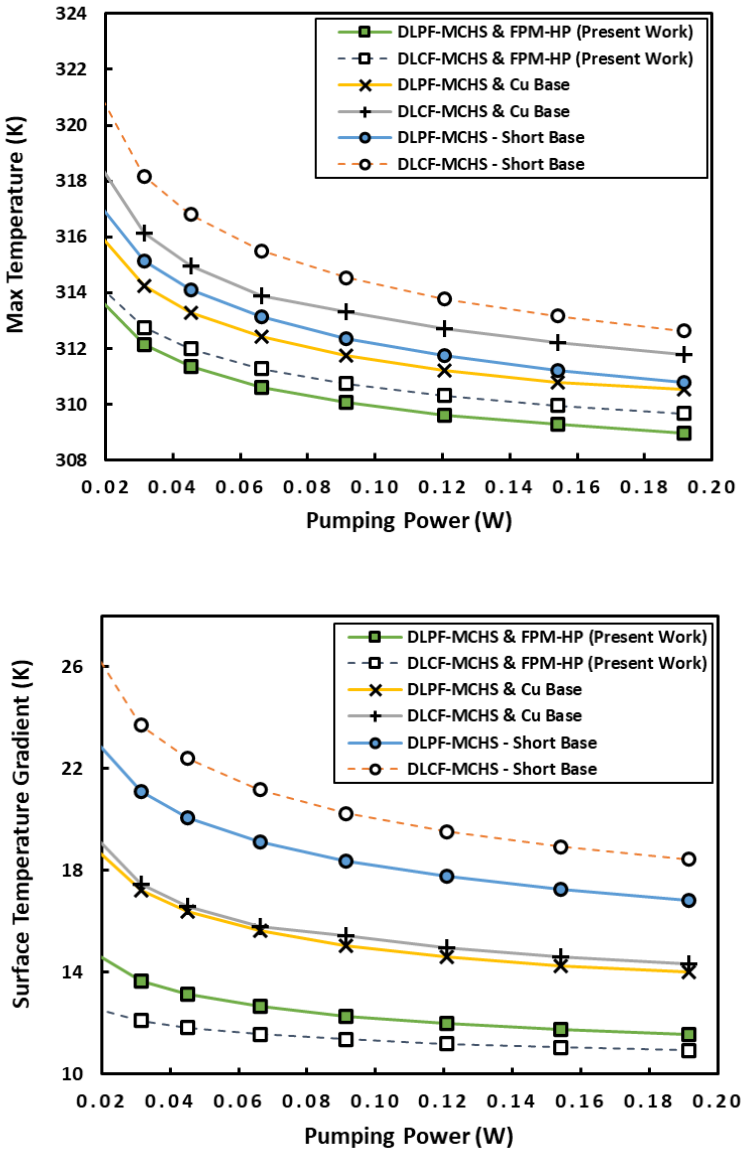

Figure 3-14 Comparison of the maximum temperature and the cooling surface temperature gradient of the studied hybrid heat sinks (Hotspot heat flux at centerline: 600 W/cm^2, Background heat flux: 100 W/cm^2).

3.5 Conclusions

Innovative hybrid heat sink designs that combine MCHS and FPM-HP technologies are optimized to improve thermal and hot spot management in electronic cooling applications with local high heat generation at the base. The hybrid heat sink is investigated for both parallel and counter flow configurations. The studied cases include cooling of electronic substrate that generates 100 W/cm2 as background heat flux and high local heat flux of 600-1000 W/cm2 at the centerline of the base. The performance of the hybrid heat sinks is compared with double-layer MCHSs with a copper heat spreader at the base and with no heat spreader at all (short base). The heat sinks' maximum temperature and surface temperature gradient at various pumping powers are compared. The results show that the trend of improvements remains consistent for both the 600 and 1000 W/cm^2 cases of hotspot heat flux. The following conclusions were corroborated within the scope of this work.

- The hybrid heat sinks combined with MCHS & FPM-HP proposed and investigated in this work have the lowest maximum temperature and surface temperature gradient among all the studied designs.
- Hybrid parallel flow configuration has an improved maximum temperature, compared to counter flow configuration ones. However, the hybrid counter flow arrangements are superior in terms of temperature uniformity at the base.
- The hybrid DLPF-MCHS & FLM-HP has the lowest maximum temperature followed by the hybrid heat sinks with DLCF and with Counter Dual Rectangular MCHSs compared to the rest of the studied heat sinks. While the hybrid Counter

Dual MCHS & FPM-HP has the lowest surface temperature gradient followed by the hybrid heat sinks with DLCF and with Counter Dual Triangular MCHSs.

- The hybrid DLPF-MCHS & FPM-HP reduces the maximum temperature and surface temperature gradient of the heat sink by 13-23% and 20-49%, while these are reduced by 16-40% and 27-64% for the DLCF-MCHS & FPM-HP compared with the corresponding copper base (no heat pipe) designs. The hybrid Counter Dual Rectangular MCHS & FPM-HP reduces the maximum temperature and surface temperature gradient of the heat sink by 15-24% and 29-65%, while these are reduced by 10-26% and 24-63% for the Counter Dual Triangular MCHS, respectively, compared with the DLCF MCHS with copper base (no heat pipe) design.
- The vapor and liquid velocity field in the heat pipes attached to the counter flow MCHSs are similar in trend and magnitude. In all studied hybrid heat sinks, the heat pipe's bottom surface acts as an evaporator, and its top surface acts as a condenser section.
- Two sets of coolant circulating loops occur mainly in the heat pipes in this study. The primary circulating loops occur in the vertical cross-sections (xy planes). The local high heat source at the center of the heat pipe base imposes secondary circulating loops of the water which occur from the bottom center of the heat pipe to the top right and top left side of the heat pipe.
- The secondary coolant circulating loop to one side of the heat pipe is more significant than the other, due to the asymmetric nature of the cooling in the MCHS,

with coolant temperature rising in the flow direction. This difference is more significant in the parallel flow MCHS which is much colder close to the inlet side than the counter flow arrangement. This result emphasizes the capability of the heat pipes to operate well in asymmetrical heating and cooling load conditions.

References

[1] Zohuri, B., “Heat Pipe Design and Technology”, Modern Application for Practical Thermal Management, Second Edition, Springer, (2016).

[2] Vafai, K., and Wang, W., “Analysis of Flow and Heat Transfer Characteristics of an Asymmetrical Flat Plate Heat Pipe”, Int. J. Heat Mass Transfer (1992), Vol. 35(9), pp. 2087–2099.

[3] Vafai, K., Zhu, N., and Wang, W., “Analysis of Asymmetric Disk-Shaped and Flat-Plate Heat Pipes”, ASME J. Heat Transfer-Trans. (1995), 117(1), pp. 209–218.

[4] Wang, Y., Vafai, K., “An Experimental Investigation of the Thermal Performance of an Asymmetrical Flat Plate Heat Pipe”, Int. J. Heat Mass Transfer (2000), 43(15), pp. 2657–2668.

[5] Zhu, N., Vafai, K., “Vapor and Liquid Flow in an Asymmetrical Flat Plate Heat Pipe: A Three-Dimensional Analytical and Numerical Investigation”, Int. J. Heat Mass Transfer (1998), 41(1), pp. 159–174.

[6] Vafai, K., and Zhu, N., “Closure to “Analysis of Asymmetric Disk-Shaped and Flat-Plate Heat Pipes”, ASME J. Heat Transfer-Trans. (2014), 136(11), p. 116001.

[7] Vafai, K., Tien, C. L., “Boundary and Inertia Effects on Flow and Heat Transfer in Porous Media”, Int. J. Heat Mass and Transfer (1980), Vol. 24, pp. 195-20.

[8] Huang, L., El-Genk, M., Tournier, J.-M., “Transient performance of an inclined water heat pipe with a screen wick”, Heat Pipes and Capillary Pumped Loops HTD (1993), 236, 87–92.

[9] Zhu, N., & Vafai, K., Analysis of cylindrical heat pipes incorporating the effects of liquid–vapor coupling and non-Darcian transport - A closed form solution. International Journal of Heat and Mass Transfer (1999), 42(18), 3405–3418.

[10] Sanhan, W., Vafai, K., K.-Lue, N., Terdtoon, P., Sakulchangsatjatai, P., “Numerical simulation of flattened heat pipe with double heat sources for CPU and GPU cooling application in laptop computers”, Journal of Computational Design and Engineering (2021), 8(2), 524–535.

[11] M. Ahmadian-Elmi,M. R. Hajmohammadi,S. S Nourazar,K. Vafai &M. B. Shafii, “Effect of filling ratio, number of loops, and transverse distance on the performance of pulsating heat pipe in a microchannel heat sink”, Numerical Heat Transfer (2023).

[12] H. Y. Noh and S. J. Kim, “Numerical simulation of pulsating heat pipes: Parametric investigation and thermal optimization,” Energy Convers. Manag., vol. 203, p. 112237 (2020).

[13] Ru J, Kong B, Zhu H, Shi Z, Zhang D, Fan T., “Microstructure, capillary performance and gas permeability of Biporous copper fabricated by tape casting”, Powder Technol 256:182–187 (2014).

[14] Maneemuang, S., Vafai, K., Kammuang-Lue1, N., Terdtoon, P., Sakulchangsatjatai, P., “Analysis of the optimum configuration for the capillary rise and the permeability of the fiber wick structure for heat removal in heat pipes”, Heat and Mass Transfer (2021) 57:1513–1526.

[15] V. S. Nikolayev, “Physical principles and state-of-the-art of modeling of the pulsating heat pipe: a review,” Appl. Therm. Eng., vol. 195, p. 117111 (2021).

Chapter 4

4.1 Conclusions

Effective thermal management in electronic components is essential, especially as these devices become more compact and powerful. In this work, innovative heat sink designs are proposed and optimized to improve thermal management in electronic components. The three-dimensional finite volume method is used to analyze the fluid flow and heat transfer in the heat sinks. The main findings and conclusions are presented below.

1. Within the scope of this study, the three-dimensional finite volume method has been demonstrated to be reliable and accurate through comparisons with experimental data.
2. The Silicon-Water Counter Dual MCHS with rectangular cross-section, investigated in this study, reduces the surface temperature gradient of the heat sink by 43-50% and 26-31% compared to DL MCHSs with parallel and counter flow configuration, respectively. The triangular cross-section reduces it by 38-47% for parallel and 21-26% for counter flow arrangement, respectively.
3. The studied Counter Dual MCHSs reduce the thermal resistance of heat sinks by 10-15% compared to DL-MCHS with parallel flow arrangement and by 2-8% compared to counter flow arrangement one.
4. The trend of improvement in thermal performance of Copper-Water MCHSs is similar to Silicon-Water ones.

5. At the studied flow rates between 50-400 ml/min, Counter Dual MCHSs with rectangular and triangular cross-section require up to 15% and 30-40% less pumping power, respectively.
6. The Counter Dual MCHSs achieve the highest Reynolds number among the studied MCHS designs.
7. At a constant channel cross-sectional area, the thermal resistance and maximum temperature of the MCHS decrease with an increase in aspect ratio of the channels, until the aspect ratio reaches 3. After that point, increasing the aspect ratio has no further impact on thermal resistance.
8. Consistent trend is observed for the change of thermal resistance and surface temperature gradient of the Counter Dual Triangular MCHS as the pumping power is varied.
9. Hybrid thermal management solutions combined with micro heat pipes show great potential for enhancing the reliability and performance of electronic devices. They are particularly useful in managing hotspots in electronic cooling applications that involve high heat generation in localized areas.
10. The hybrid heat sinks combined with MCHS & FPM-HP have the lowest maximum temperature and surface temperature gradient compared to all other designs studied. This proves that the combination of MCHSs and FPM-HPs is an effective solution for achieving optimal cooling performance.

11. Hybrid parallel flow configuration displays better maximum temperature than those with counter flow configuration. However, hybrid counter flow arrangements are superior in achieving uniformity of temperature at the base.
12. The hybrid DLPF-MCHS & FPM-HP has the lowest maximum temperature followed by the hybrid heat sinks with DLCF and with Counter Dual Rectangular MCHSs compared to the rest of the studied heat sinks. While the hybrid Counter Dual MCHS & FPM-HP has the lowest surface temperature gradient followed by the hybrid heat sinks with DLCF and with Counter Dual Triangular MCHSs.
13. The hybrid DLPF-MCHS & FPM-HP reduces the maximum temperature and surface temperature gradient of the heat sink by 13-23% and 20-49%, while these are reduced by 16-40% and 27-64% for the DLCF-MCHS & FPM-HP compared with the corresponding copper base (no heat pipe) designs. The hybrid Counter Dual Rectangular MCHS & FPM-HP reduces the maximum temperature and surface temperature gradient of the heat sink by 15-24% and 29-65%, while these are reduced by 10-26% and 24-63% for the Counter Dual Triangular MCHS, respectively, compared with the DLCF MCHS with copper base (no heat pipe) design.
14. In all studied hybrid heat sinks, the heat pipe's bottom surface acts as an evaporator, and its top surface acts as a condenser section.
15. The vapor and liquid velocity field in the heat pipes attached to the counter flow MCHSs are similar in trend and magnitude.

16. The heat pipes in this study had two sets of coolant circulating loops. The first set occurred in the vertical cross-sections (xy planes), while the second set was imposed by the local high heat source at the center of the heat pipe base. The secondary circulating loops caused the water to flow from the bottom center of the heat pipe to the top right and top left side of the heat pipe.
17. The asymmetrical nature of cooling in the MCHS (with coolant temperature rising in the flow direction) causes one side of the heat pipe's secondary coolant circulating loop to be more significant than the other. This difference is especially noticeable in the parallel flow MCHS, which is much colder near the inlet side than in the counter flow arrangement. This highlights the heat pipes' ability to function effectively under uneven heating and cooling loads.
18. The use of hybrid MCHS & FPM-HP shows a consistent trend of improvements in both the 600 and 1000 W/cm^2 cases of hotspot heat flux.